arXiv:1603.05502v2 [hep-ph] 27 Sep 2016

HRI-RECAPP-2016-006

Revisiting the Exclusion Limits from Direct Chargino-Neutralino Production at the LHC

Arghya Choudhury[a,b1] Subhadeep Mondal[c2]

[a]Consortium for Fundamental Physics, Department of Physics and Astronomy, University of Sheffield, Sheffield S3 7RH, United Kingdom

[b]Consortium for Fundamental Physics, Department of Physics and Astronomy, University of Manchester, Manchester, M13 9PL, United Kingdom

[c] Regional Centre for Accelerator-based Particle Physics, Harish-Chandra Research Institute, Jhusi, Allahabad - 211019, India

Abstract

We revisit the existing limits on the gaugino masses in various Supersymmetric (SUSY) scenarios derived from Run-I data of the LHC. These limits obtained from the various final states rely heavily on the simplified assumptions regarding the masses, compositions and decay branching ratios of the gauginos. The most severe exclusion limits on the gaugino masses are obtained from trilepton final states while the second lightest neutralino ($\widetilde{\chi}_2^0$) decaying into the SM-like Higgs and lightest SUSY particle (LSP) results in the weakest bounds. Our aim is to assess the extent of deviation of these exclusion limits in more realistic scenarios. After a brief discussion on the various decay modes of the $\widetilde{\chi}_2^0$ and the lightest chargino ($\widetilde{\chi}_1^\pm$), we proceed to validate the ATLAS exclusion limits obtained from trilepton, $l\gamma\gamma$ and $lb\bar{b}$ final states associated with missing energy. We then consider different combinations of the relevant branching ratios to study their impact on the existing bounds. The results are presented alongside the existing exclusion limits to showcase the extent of the obtained deviation. We also observe that the three-body decay modes of $\widetilde{\chi}_2^0$ and $\widetilde{\chi}_1^\pm$ via off-shell slepton decays resulting in trilepton final states provide bounds that are far more severe in some parts of the available parameter space than that obtained from the off-shell gauge boson decays.

[1]a.choudhury@sheffield.ac.uk

[2]subhadeepmondal@hri.res.in

Contents

1 Introduction **2**

2 Probing the Electroweak Sector **5**

2.1 $\widetilde{\chi}_2^0$ decay modes 7

2.1.1 Impact of sign of μ 10

2.2 $\widetilde{\chi}_1^\pm$ decay modes 11

2.3 Impact of $(g-2)_\mu$ 13

2.4 Benchmark Points 14

3 Collider Analysis **16**

3.1 Search for Trilepton final states 16

3.2 Search for final states with Higgs 19

3.2.1 One lepton and two b-jets channel 19

3.2.2 One lepton and two photons channel 21

3.3 Revisiting the exclusion limits with varying branching ratios 22

4 Summary and Conclusions **27**

1 Introduction

After a long shutdown, the Large Hadron collider (LHC) is now operating in full swing at a center of mass energy, $\sqrt{s} = 13$ TeV. In the aftermath of its huge success in terms of the discovery of the elusive Higgs boson with mass around 125 GeV [1, 2] , the prime goal of Run-II now is to look for new physics beyond the Standard Model (BSM). So far, after analysing the Run-I data, ATLAS and CMS have only reported some small inconclusive local excesses [3, 4] over the SM predictions, which need to be put under thorough scrutiny at Run-II. Any of these excesses, if proven significant, will open the window to the hitherto

unknown BSM physics. On the other hand, after just a few months of data accumulation at $\sqrt{s} = 13$ TeV, both CMS and ATLAS have hinted towards a possible scalar resonance at 750 GeV [5, 6] that has created a lot of buzz within the particle physics community. Although promising, one has to wait for more data and finer analyses to ascertain if this is indeed the first hint of the BSM physics we are so eagerly waiting for. At this stage, it is therefore worthwhile to look back to our favourite new physics models and revisit the exclusion limits derived from the existing experimental data. Supersymmetry (SUSY) [7–9], being one the frontrunners among the BSM candidates, has been searched for extensively both by the ATLAS and the CMS. The experimental results so far indicate towards a heavy coloured sector *(strongly interacting sector)* within the framework of the minimal supersymmetric SM (MSSM) [10–12]. ATLAS and CMS have already excluded first two generation squarks and gluino masses upto 1.7 TeV for degenerate squark-gluino scenario [10–12] [1] from Run-I data. Depending upon the scenarios, the very recent Run-II data with an integrated luminosity $(\mathcal{L}) = 3.2$ fb^{-1}, the limit on gluino and squarks has already been increased by 100 to 200 GeV [14, 15].

At the same time, exclusion limits on the masses of the electroweak sector sparticles, namely, charginos, neutralinos [2] and sleptons, are *much* weaker because of their relatively smaller production cross-sections at the LHC. The stringent limits on the coloured sector sparticles make the search of the electroweakinos and the sleptons all the more important from the perspective of SUSY searches at the 13 and 14 TeV run of the LHC. As the ATLAS and the CMS collaborations have not yet published any new search results of the electroweak sparticles from the very first 13 TeV 3.2 fb^{-1} data, here we will only focus on the Run-I data and the corresponding limits. From the combined data obtained at 7 TeV and 8 TeV runs, the experimental collaborations have already put significant mass limits on the electroweakinos and the sleptons from direct search channels [16–22] that include chargino - neutralino, chargino pair and slepton pair productions. However, the existing bounds apply only for some simplified SUSY scenarios which assume a certain hierarchy between the slepton and the gaugino masses and also fix their compositions. In the studies of the electroweakinos, for example, the lightest neutralino ($\widetilde{\chi}_1^0$) which is also assumed to be the lightest supersymmetric particle (LSP) is usually supposed to be purely bino-like while the second lightest neutralino ($\widetilde{\chi}_2^0$) and the lighter chargino ($\widetilde{\chi}_1^\pm$) are purely wino-like [16–22]. These assumptions have crucial impact on the relevant production cross-section and decay branching ratio (BR) of the concerned sparticle and as a result, the existing bounds are

[1] However, these strong bounds reduce significantly in compressed SUSY type scenarios [13].

[2] In this paper we will refer to the charginos and neutralinos as the electroweakinos.

expected to change significantly in more realistic scenarios.

The most stringent bound on chargino - neutralino mass plane is obtained from $\widetilde{\chi}_1^{\pm}\widetilde{\chi}_2^0$ pair production leading to various trilepton + transverse missing energy ($\not{E}_{\rm T}$) final states [16,22]. A number of phenomenological studies already exist which have analysed the implications of electroweakino searches and related topics at the LHC [23–27]. In a recent work [25] it has been shown that the LHC constraints in the trilepton channel are significantly weaker even in the presence of light sleptons ($m_{\widetilde{l}} < m_{\widetilde{\chi}_1^{\pm}}$), especially in the models with higgsino dominated $\widetilde{\chi}_1^{\pm}, \widetilde{\chi}_2^0$ and $\widetilde{\chi}_3^0$; compared to the scenarios mostly studied by the LHC collaborations with wino-dominated $\widetilde{\chi}_1^{\pm}, \widetilde{\chi}_2^0$. For such scenarios with higgsino dominated gauginos (or gauginos with non-negligible higgsino component) Br($\tilde{\chi}_3^0, \tilde{\chi}_2^0 \to h\tilde{\chi}_1^0$) is usually large and as a consequence reduces the signal significance of the trilepton final states. Even for wino-dominated $\widetilde{\chi}_1^{\pm}$ and $\widetilde{\chi}_2^0$ and with decoupled sleptons, the limits obtained by ATLAS and CMS are much weaker when $\widetilde{\chi}_2^0$ decays via $Z\widetilde{\chi}_1^0$. One obtains the weakest exclusion limits when $\widetilde{\chi}_2^0$ decays via the *spoiler* mode ($h\widetilde{\chi}_1^0$) [3] [19, 20, 22]. In the decoupled - sleptons scenarios, the subsequent two body decays $\widetilde{\chi}_1^{\pm} \to \widetilde{\chi}_1^0 W^{\pm}$ and $\widetilde{\chi}_2^0 \to \widetilde{\chi}_1^0 Z/h$ result in various leptonic final states associated with b-jets or photons and $\not{E}_{\rm T}$. ATLAS collaboration has recently presented the electroweakino search results with $1l + 2b$ and $1l + 2\gamma$ final states [19]. However, the limits are derived on the gaugino mass plane assuming 100% branching ratio into one particular decay mode, which does not provide us with the whole picture. The interplay between the two-body decay modes like ($\widetilde{\chi}_2^0 \to h\widetilde{\chi}_1^0$ and $\widetilde{\chi}_2^0 \to Z\widetilde{\chi}_1^0$) can also modify the exclusion limits considerably in more realistic situations, e.g., phenomenological MSSM (pMSSM) [28]. It is, therefore, worthwhile to revisit the existing limits with different compositions and mass hierarchies of the gauginos. Moreover, the off-shell production and subsequent decays of the gauge bosons and sleptons from $\widetilde{\chi}_2^0/\widetilde{\chi}_1^{\pm}$ decays can result in a wide range of possible decay BRs. These off-shell decay modes, if taken into account, can also give rise to similar final states as obtained from the two-body decay modes of the gauginos. All these possibilities need to be explored in the light of the data accumulated from run-I before embarking to the run-II of the LHC.

A light gaugino and (or) slepton scenario is also highly motivated from the observed excess of anomalous magnetic moment of muon ($(g-2)_\mu$) measurements and existence of Dark Matter (DM). In order to fit the excess in $(g-2)_\mu$ [29] over the SM predictions within the framework of MSSM, requires the slepton and the lighter chargino masses in the few hundreds of GeV range [24, 25, 30]. Various leptonic final states associated with large missing energy are the favoured channels to look for such a scenario. A heavy coloured

[3] A few phenomenological analyses in this context may be seen in Ref. [25–27].

sector, as favoured by the LHC data, fits more naturally for such MSSM parameter space as their contributions to the cascade of the gauginos from even off-shell productions are small in that case resulting in larger branching ratios to the leptonic final states resulting in cleaner signals. In all R-parity conserving SUSY models, the LSP (in our case, $\widetilde{\chi}_1^0$) is stable and can be a good candidate for the elusive dark matter (DM) [31–33] in the universe. A partial list of works on supersymmetric DM may be seen in Ref. [34–39]. The electroweak sparticles may also lead to correct relic density for DM via the DM annihilation/coannihilation mechanisms. This way the electroweak sector can also be constrained from the precisely measured value of DM relic density by WMAP [40] or PLANCK [41].

In this present study, we assume that the sleptons are heavier than the electroweakinos, but not so heavy that they may be considered to be decoupled. The entire coloured sector, on the other hand, is decoupled from the rest of the SUSY spectrum. Apart from the obvious advantages of having light sleptons in the theory from the viewpoint of $(g-2)_\mu$ and DM, such scenarios may result in significant enhancement of the three body branching ratios of the electroweakinos from the off-shell decays of the sleptons. Such off-shell slepton decays in this context of the gauginos have not been studied by the experimental collaborations so far.

The paper is organised in the following way. First, we explore the available parameter space in pMSSM through a detailed scan using the constraints derived from the most updated collider and flavour physics data. In Sec. 2 we discuss about the various decay modes of $\widetilde{\chi}_2^0$ and $\widetilde{\chi}_1^\pm$ with different slepton-gaugino mass hierarchies to study the variation of their various 2-body and 3-body decay branching ratios. Here we also briefly discuss about the impact of muon g-2 and DM relic density on the available parameter space. In Sec. 3, we study the direct pair production of $\widetilde{\chi}_2^0\widetilde{\chi}_1^\pm$ and their subsequent decays resulting in various final states following the footsteps of the corresponding ATLAS analyses for validation. Then we proceed with the same scenarios with different values of the 2-body and 3-body branching ratios of $\widetilde{\chi}_2^0$ and $\widetilde{\chi}_1^\pm$ to produce similar final states and revisit the present exclusion limits imposed by the ATLAS analyses. We finally provide our conclusions in Sec. 4.

2 Probing the Electroweak Sector

In this section, first we briefly discuss about the various two-body and three-body decay modes of $\widetilde{\chi}_2^0$ and $\widetilde{\chi}_1^\pm$ to study the interplay among the branching ratios for different choices of gaugino compositions and slepton - gaugino mass hierarchies. In the simplified model scenarios, the exclusion limits on the gaugino masses are derived assuming both $\widetilde{\chi}_2^0$ and $\widetilde{\chi}_1^\pm$

decay into any one of their respective available two-body decay modes with 100% branching ratio. Our aim is to find combinations of different decay modes of these particles that also may give rise to similar final states. Therefore, in order to obtain a clear idea of the variation of the branching ratios of $\widetilde{\chi}_2^0$ and $\widetilde{\chi}_1^\pm$ over the pMSSM parameter space, we scan the relevant parameters in the following ranges:

$$1 \text{ GeV} < M_1 < 1200 \text{ GeV}, \quad 100 \text{ GeV} < M_2 < 1500 \text{ GeV}, \quad 100 \text{ GeV} < \mu < 2000 \text{ GeV}$$
$$1 < \tan\beta < 50, \quad 100 \text{ GeV} < M_{l_L} < 2000 \text{ GeV}, \quad 100 \text{ GeV} < M_{l_R} < 2000 \text{ GeV},$$

where, M_1, M_2 and μ are the bino, wino and higgsino soft mass parameters respectively. $\tan\beta$ is the ratio of the up-type and down-type Higgs vacuum expectation values. M_{l_L} and M_{l_R} denote the left and right-handed slepton soft masses respectively. We assume equal soft masses for all three generations sleptons. The gluino and the squark sector particles have no impact in our present study. Hence we decouple these particles from the rest of the spectrum and keep their soft mass parameters at 3 TeV. For this scan we have used SUSPECT [42] and SUSY-HIT [43] to calculate the SUSY spectrum and the relevant branching ratios. The flavour and other low energy constraints have been calculated using micrOMEGAs [44]. While scanning we ensure that for all the points $M_1 < M_2 < \mu$, so that the LSP is always mostly bino-like. However, since M_1, M_2 and μ have all been varied independent of each other, the LSP may as well be a bino-wino or bino-wino-higgsino mixed state. We also make sure that for all our points, $\widetilde{\chi}_1^\pm$ (mostly wino-like) is the NLSP. As a result of our choice of the gaugino mass parameters, the $\widetilde{\chi}_1^\pm$ is either wino-like or a wino-higgsino mixed state. $\widetilde{\chi}_2^0$ is also mostly expected to be wino-like and have a mass close to that of $\widetilde{\chi}_1^\pm$. However, it may also be a wino-bino, wino-higgsino or wino-bino-higgsino mixed state. As a consequence of having $\widetilde{\chi}_1^\pm$ (and $\widetilde{\chi}_2^0$ if these masses are degenerate), as NLSP, none of $\widetilde{\chi}_2^0$ or $\widetilde{\chi}_1^\pm$ can decay into an on-shell slepton or sneutrino. However, these sfermions can be produced off-shell and the three body decay modes of the electroweakinos may have large enough branching ratios which can not be ignored. We discuss more about this later in this section. The following experimental constraints have been taken into account while scanning:

- The lightest CP-even Higgs boson mass should be in the range 125 $\pm$3 GeV [1, 2] considering a theoretical uncertainty of 3 GeV [45].
- Lighter chargino ($\widetilde{\chi}_1^\pm$) mass should be above LEP exclusion limit, i.e, 103.5 GeV [46].
- We impose the flavour physics constraints:
  $2.82 \times 10^{-4} < \text{BR}(b \to s\gamma) < 4.04 \times 10^{-4}$ (at 2σ level) [47] and
  $1.57 \times 10^{-9} < \text{BR}(B_s \to \mu^+\mu^-) < 4.63 \times 10^{-9}$ (at 2σ level) [47].

- Limits on slepton masses: Both ATLAS and CMS have looked for sleptons via direct production channels with di-lepton final states associated with $\not{E}_T$ [17]. In these analyses sleptons are considered as NLSP and BR($\widetilde{l} \to l\widetilde{\chi}_1^0$) = 100%. For example, with degenerate Left(L) and Right(R) type slepton masses, LHC data exclude the region $90 < m_{\widetilde{l}} < 325$ GeV for a massless LSP. As the LSP-slepton mass splitting decreases, the exclusion limit becomes weaker. Again only for L-type or R-type slepton production, the exclusion limit is relatively weaker than the degenerate case (see Fig. 8 of Ref. [17]). In our parameter space scan, $\widetilde{\chi}_1^\pm$ and $\widetilde{\chi}_2^0$ are always assumed to be lighter than the sleptons. In most of the regions, R-type sleptons dominantly decay to $l\widetilde{\chi}_1^0$, but the L-type sleptons can have significant branching ratio in the additional decay modes like $\nu\widetilde{\chi}_1^\pm$ or $l\widetilde{\chi}_2^0$ which have not been considered by the LHC collaborations. In such scenarios, limits on the slepton (L-type) masses can change from the existing limits. A detailed computation of these revised limits is beyond the scope of this work. Instead, we have implemented the bounds on the slepton masses in a bin-by-bin basis separately for L-type and R-type sleptons derived from Fig. 8 of Ref. [17] depending on various slepton and LSP mass regions.

2.1 $\widetilde{\chi}_2^0$ decay modes

The dominant two-body decay modes of the second lightest neutralino ($\widetilde{\chi}_2^0$) are $\widetilde{\chi}_2^0 \to \widetilde{\chi}_1^0 h$, $\widetilde{\chi}_2^0 \to \widetilde{\chi}_1^0 Z$ and $\widetilde{\chi}_2^0 \to f\widetilde{f}$, where h denotes the SM-like lightest CP even Higgs boson[4] and $f(\widetilde{f})$ denotes the fermions (sfermions). If the squarks and sleptons in the theory are heavier than $\widetilde{\chi}_2^0$, depending on the mass difference between $\widetilde{\chi}_2^0$ and $\widetilde{\chi}_1^0$ ($\Delta m^0_{\widetilde{\chi}}$), any one of the other two decay modes dominate or compete with each other.

In Fig. 1, we show the distribution of the branching ratios of the two 2-body decay modes of the $\widetilde{\chi}_2^0$ into h and Z final states associated with $\widetilde{\chi}_1^0$. The distributions are shown as a function of the $\widetilde{\chi}_2^0$ mass ($m_{\widetilde{\chi}_2^0}$). Effect of the mass difference, $\Delta m^0_{\widetilde{\chi}}$ on the BR of these decay modes can be understood by the different colours and shapes of the points. We take different mass windows of $\Delta m^0_{\widetilde{\chi}}$ to showcase the effect. The magenta points correspond to $\Delta m^0_{\widetilde{\chi}} > 200$ GeV. For such a large mass difference, both the decay modes are open. However, in this case, BR($\widetilde{\chi}_2^0 \to h\widetilde{\chi}_1^0$) > BR($\widetilde{\chi}_2^0 \to Z\widetilde{\chi}_1^0$). This is due to the fact that the Z boson only couples with the neutralinos via their higgsino components. Higgsino components in both the $\widetilde{\chi}_1^0$ and the $\widetilde{\chi}_2^0$ states being small in most of the points, this decay mode is generally suppressed compared to the other. The blue circle points correspond to $125 < \Delta m^0_{\widetilde{\chi}} < 200$

[4]We assume all the other Higgs bosons in the MSSM are decoupled from rest of the spectrum.

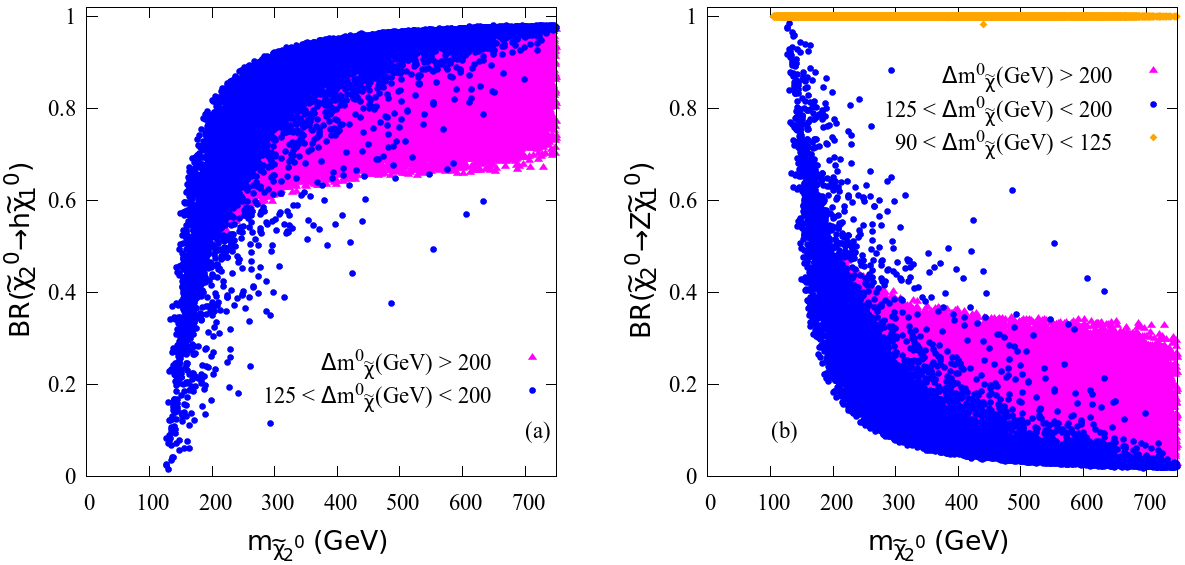

Figure 1: Distributions of the BR's corresponding to the two 2-body decay modes of $\widetilde{\chi}_2^0$ shown as a function of $m_{\widetilde{\chi}_2^0}$. The left plot (a) shows the distributions of BR($\widetilde{\chi}_2^0 \to h\widetilde{\chi}_1^0$) and the right plot (b), that of BR($\widetilde{\chi}_2^0 \to Z\widetilde{\chi}_1^0$). The different coloured points in the plots correspond to the different $\Delta m^0_{\widetilde{\chi}} = m_{\widetilde{\chi}_2^0} - m_{\widetilde{\chi}_1^0}$ as indicated in the plot.

GeV. Again we obtain similar pattern except for the points where the mass difference is barely sufficient to produce h in the final state. Once there is enough phase space for the decay, $\widetilde{\chi}_2^0 \to h\widetilde{\chi}_1^0$ to take place, its BR starts to dominate. Orange triangle points in Fig. 1b correspond to $90 < \Delta m^0_{\widetilde{\chi}} < 125$ GeV. Naturally, the $\widetilde{\chi}_2^0$ decays entirely to $Z\widetilde{\chi}_1^0$ mode as the other decay mode is kinematically inaccessible.

Fig. 2 shows the distribution of the BRs of the three 3-body decay modes of $\widetilde{\chi}_2^0$ into different leptonic final states. Once the two-body decay modes become kinematically inaccessible, these three-body decays start to show up. The contribution to these decay modes may come from off-shell sleptons as well as off-shell Z or h decays. To determine how heavy sleptons affect these decays, we have plotted the BRs as a function of $m_{\widetilde{\chi}_2^0}$ corresponding to different mass ranges of $\Delta m_{\widetilde{l}_{L/R}/\widetilde{\nu}_L/\widetilde{\tau}_1} = m_{\widetilde{l}_{L/R}/\widetilde{\nu}_L/\widetilde{\tau}_1} - m_{\widetilde{\chi}_2^0}$ denoting them by different colored points. While plotting BR($\widetilde{\chi}_2^0 \to l\bar{l}\widetilde{\chi}_1^0$), the $\widetilde{l}$ - $\widetilde{\chi}_2^0$ mass gap is calculated by choosing the smaller mass between $m_{\widetilde{l}_L}$ or $m_{\widetilde{l}_R}$ as the slepton mass since both the L-type or the R-type sleptons may affect the branching ratio. Note that, BR($\widetilde{\chi}_2^0 \to l\bar{l}\widetilde{\chi}_1^0$) includes both electron and muon final states. However, while plotting BR($\widetilde{\chi}_2^0 \to \nu\bar{\nu}\widetilde{\chi}_1^0$), we only consider different ranges of $\Delta m_{\widetilde{\nu}_L}$. BR($\widetilde{\chi}_2^0 \to \nu\bar{\nu}\widetilde{\chi}_1^0$) includes sum of all the three neutrino decay modes. For BR($\widetilde{\chi}_2^0 \to \tau\bar{\tau}\widetilde{\chi}_1^0$), we consider $\Delta m_{\widetilde{\tau}_1}$. As seen from the plots, off-shell slepton decays contribute mostly while

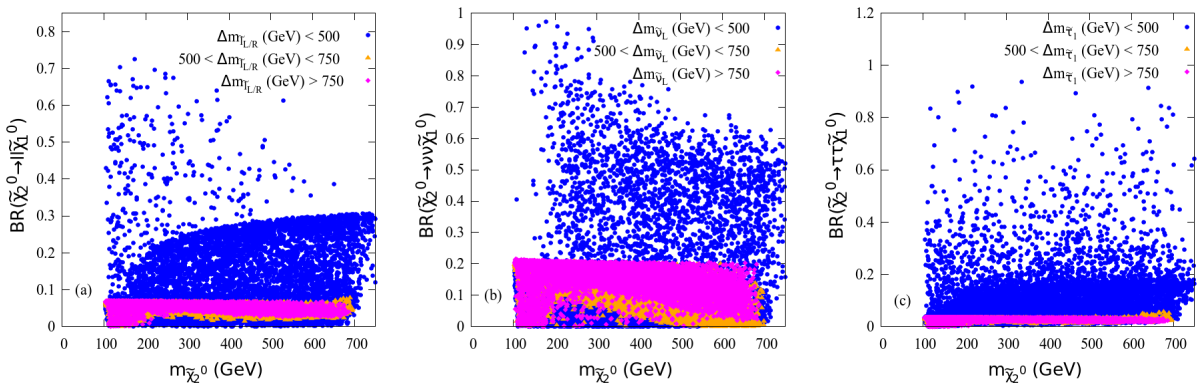

Figure 2: Distributions of the BR's corresponding to the three leptonic 3-body decay modes of $\widetilde{\chi}_2^0$ shown as a function of $m_{\widetilde{\chi}_2^0}$. The plots show the distributions corresponding to BR($\widetilde{\chi}_2^0 \to l\bar{l}\widetilde{\chi}_1^0$) in left (a), BR($\widetilde{\chi}_2^0 \to \nu\bar{\nu}\widetilde{\chi}_1^0$) in middle (b) and BR($\widetilde{\chi}_2^0 \to \tau\bar{\tau}\widetilde{\chi}_1^0$) in right (c) respectively. Note that, BR($\widetilde{\chi}_2^0 \to l\bar{l}\widetilde{\chi}_1^0$) contains contributions from both the electron and muon associated final states while BR($\widetilde{\chi}_2^0 \to \nu\bar{\nu}\widetilde{\chi}_1^0$) contains all the three neutrino flavour contributions. The different coloured (shaped) points correspond to the different $\Delta m_{\widetilde{l}_{L/R}/\widetilde{\nu}_L/\widetilde{\tau}_1} = m_{\widetilde{l}_{L/R}/\widetilde{\nu}_L/\widetilde{\tau}_1} - m_{\widetilde{\chi}_2^0}$ (see text for details).

$\Delta m_{\widetilde{l}_{L/R}}(/\Delta m_{\widetilde{\nu}_L}/\Delta m_{\widetilde{\tau}_1}) < 500$ GeV as shown by the blue (circle) points. Naturally, we obtain highest BR for the $\tau\bar{\tau}$ final state, stau being the lightest slepton. As the slepton - $\widetilde{\chi}_2^0$ mass difference keeps increasing, contributions from off-shell sleptons start to diminish and that from off-shell Z-boson start to dominate. The Z-boson, despite being much lighter than the sleptons, only starts to affect the BRs in cases where the slepton masses are quite heavy since for most of the points both $\widetilde{\chi}_1^0$ and $\widetilde{\chi}_2^0$ has small higgsino components and hence their coupling to Z-boson is usually suppressed. Contribution of the off-shell Higgs boson state is small due to its small coupling with the SM leptons. The orange (triangle) points correspond to 500 GeV $< \Delta m_{\widetilde{l}_{L/R}}(/\Delta m_{\widetilde{\nu}_L}/\Delta m_{\widetilde{\tau}_1}) <$ 750 GeV and the magenta (diamond) points correspond to a mass difference $>$ 750 GeV. Note that, the spread in the orange and the magenta points are obtained due to the off-shell slepton contributions and the varying higgsino components in the neutralinos. Looking at the values of the BRs from the plots it can be easily understood that once the mass difference becomes greater than 500 GeV, the three body decays are entirely controlled by off-shell Z-decays. One should note that, there exist a large part of the parameter space where $\widetilde{\chi}_2^0$ has a very large branching ratio into the invisible mode ($\nu\nu\widetilde{\chi}_1^0$). None of the usual search channels are sensitive to probe such a scenario from $\widetilde{\chi}_1^{\pm}$-$\widetilde{\chi}_2^0$ pair production.

2.1.1 Impact of sign of μ

Note that, so far we have only concentrated on a positive μ while deriving our results. However, reversing the sign of μ may alter the results significantly. It is well known that the decay width of $\widetilde{\chi}_2^0 \to \widetilde{\chi}_1^0 h$ depends on the sign of μ and may go down considerably. Under certain approximations in the Higgs decoupling limit, it can be shown that this decay branching ratio is proportional to a fator $(\frac{M_1+M_2}{\mu} + \frac{4}{\tan\beta})^2$ [27]. Hence for a negative μ and $|\mu| >> M_1, M_2$, one would expect BR($\widetilde{\chi}_2^0 \to h\widetilde{\chi}_1^0$) to be suppressed than BR($\widetilde{\chi}_2^0 \to Z\widetilde{\chi}_1^0$) in that region of parameter space, where both the decay modes are open. The cancellation is even more severe as $\tan\beta$ decreases. To showcase this behavior, we show in Fig. 3, the relative strengths of the two concerned decay BR's as a function of $m_{\widetilde{\chi}_2^0}$. For this purpose, we keep the LSP bino-like with M_1 fixed at 100 GeV. Lower limit of M_2 is chosen such that both the decay modes, $\widetilde{\chi}_2^0 \to Z(h)\widetilde{\chi}_1^0$ are kinematically possible. All the sleptons and the squarks in the theory are decoupled from rest of the spectrum. μ-value is kept fixed at 1 TeV while its sign is varied. To showcase the $\tan\beta$ dependence, we choose to present our results at two $\tan\beta$ values, 10 and 30.

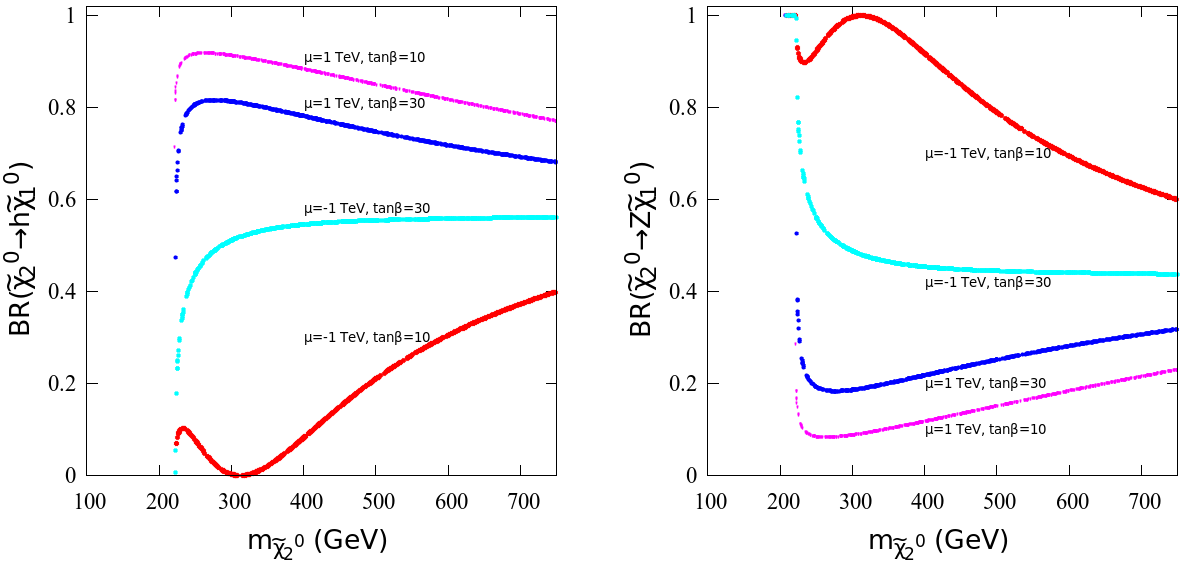

Figure 3: Distributions of the BR's corresponding to the two 2-body decay modes of $\widetilde{\chi}_2^0$ shown as a function of $m_{\widetilde{\chi}_2^0}$ for different sign of μ at a fixed LSP mass and two different $\tan\beta$ values. The left plot (a) shows the distributions of BR($\widetilde{\chi}_2^0 \to h\widetilde{\chi}_1^0$) and the right plot (b), that of BR($\widetilde{\chi}_2^0 \to Z\widetilde{\chi}_1^0$). M_1 is kept fixed at 100 GeV while all the sleptons and the squarks in the theory are decoupled.

In Fig. 3, the magenta and blue coloured points correspond to positive μ for tanβ= 10 and 30 respectively. In this case, the distribution of the BR's are similar as already depicted in Fig. 1. On the other hand, red and cyan points corresponds to negative μ for tanβ= 10 and 30 respectively. As expected, for this case, BR($\widetilde{\chi}_2^0 \to Z\widetilde{\chi}_1^0$) dominates over BR($\widetilde{\chi}_2^0 \to h\widetilde{\chi}_1^0$) even when both the decay modes are kinematically accessible. Since the magnitude of the μ-parameter ($|\mu|$) remains fixed at 1 TeV, the dominance of BR($\widetilde{\chi}_2^0 \to Z\widetilde{\chi}_1^0$) over BR($\widetilde{\chi}_2^0 \to h\widetilde{\chi}_1^0$) becomes less prominent as M_2 increases.

2.2 $\widetilde{\chi}_1^\pm$ decay modes

The sleptons in the theory being heavier than $\widetilde{\chi}_1^\pm$, it has only one two body decay mode, $\widetilde{\chi}_1^\pm \to W^\pm \widetilde{\chi}_1^0$. Therefore, if kinematically allowed, BR to this decay mode stands at 100%. Once $m_{\widetilde{\chi}_1^\pm} - m_{\widetilde{\chi}_1^0} < m_W$, the three body decay modes starts to open up.

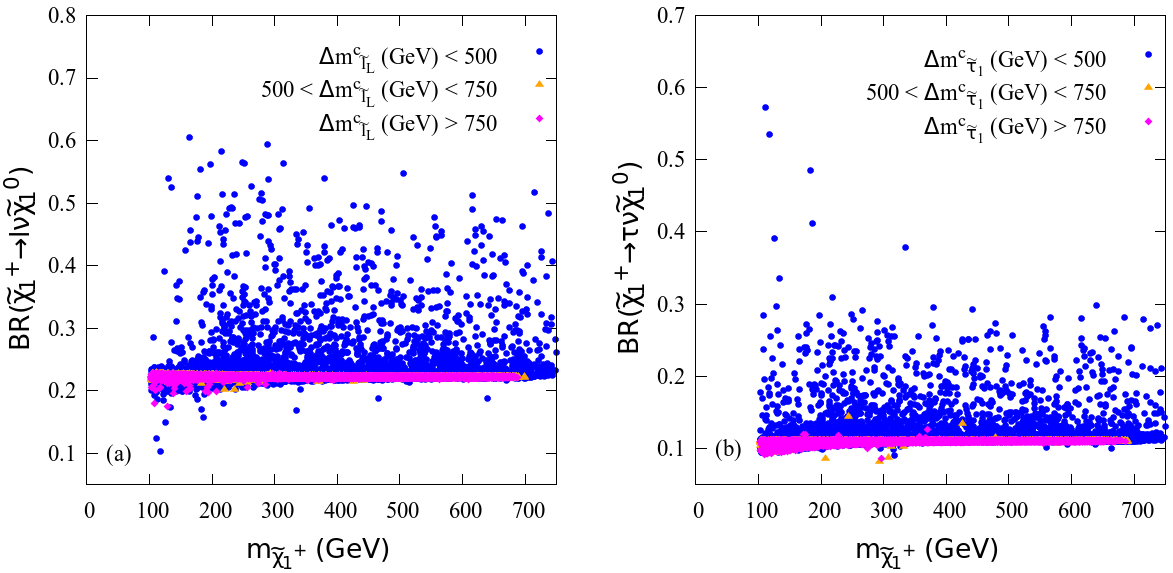

Figure 4: Distributions of the BR's corresponding to the leptonic 3-body decay modes of $\widetilde{\chi}_1^\pm$ shown as a function of $m_{\widetilde{\chi}_1^\pm}$. The left plot (a) show the distributions corresponding to BR($\widetilde{\chi}_1^\pm \to l\nu_l l\widetilde{\chi}_1^0$), and the right plot (b), that of BR($\widetilde{\chi}_1^\pm \to \tau\nu_\tau\widetilde{\chi}_1^0$). Note that, BR($\widetilde{\chi}_1^\pm \to l\nu_l l\widetilde{\chi}_1^0$) contains contributions from both the electron and muon associated final states. The different coloured (shaped) points correspond to the different $\Delta m^c_{\widetilde{l}_L/\widetilde{\tau}_1} = m_{\widetilde{l}_L/\widetilde{\tau}_1} - m_{\widetilde{\chi}_1^\pm}$.

Fig. 4 shows the distribution of the BRs of the three body decay modes of $\widetilde{\chi}_1^\pm$ into different leptonic final states. Since our $\widetilde{\chi}_1^\pm$ is mostly wino-like, it only couples with the left-handed sleptons. Hence, we showcase the effects of the slepton mass on this decay BRs by

the different coloured points in the plot corresponding to different mass ranges of $\Delta m^c_{\widetilde{l}_{L/\widetilde{\tau}_1}} = m_{\widetilde{l}_{L/\widetilde{\tau}_1}} - m_{\widetilde{\chi}_1^\pm}$. Apart from the off-shell sleptons, off-shell W-bosons may also contribute here. However, as in the case of $\widetilde{\chi}_2^0$, here also the off-shell sleptons contribute mostly toward the three-body decays unless they are too heavy. We plot BR($\widetilde{\chi}_1^\pm \to l\nu_l l\widetilde{\chi}_1^0$) as a summed up contribution of the both electron and muon associated decay modes. BR($\widetilde{\chi}_1^\pm \to \tau\nu_\tau\widetilde{\chi}_1^0$) dominates as long as the sleptons are relatively light ($\Delta m^c_{\widetilde{l}_L}$ ($\Delta m^c_{\widetilde{\tau}_1}$) < 500 GeV), shown as the blue (circle) points in the distributions. Once the sleptons start to get heavy, the off-shell W-boson starts to contribute as shown by the orange (triangle) and magenta (diamond) points, corresponding to $500 < \Delta m^c_{\widetilde{l}_L}$ ($\Delta m^c_{\widetilde{\tau}_1}$) < 750 GeV and $\Delta m^c_{\widetilde{l}_L}$ ($\Delta m^c_{\widetilde{\tau}_1}$) > 750 GeV respectively.

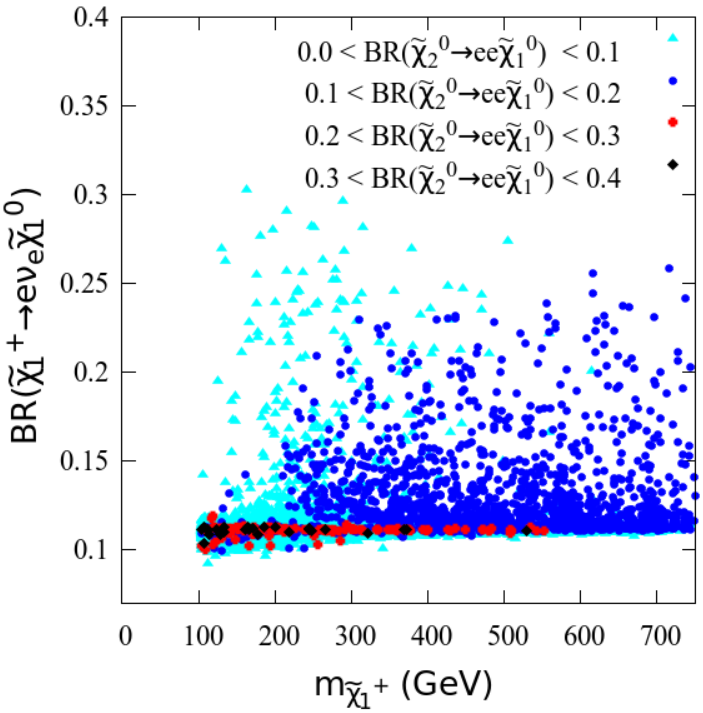

Figure 5: Distribution of BR($\widetilde{\chi}_1^\pm \to \widetilde{\chi}_1^0 e^\pm \nu_e$) shown as a function of $m_{\widetilde{\chi}_1^\pm}$. The cyan, blue, red and black points indicate BR($\widetilde{\chi}_2^0 \to \widetilde{\chi}_1^0 e^\pm e^\mp$) $< 10\%$, 10%-20%, 20%-30% and 30%-40% respectively.

The large three-body branching ratios of the gauginos in part of the parameter space indicate that comparable exclusion limits may be derived if one considers them as well instead of considering only the two-body decay modes. To emphasise this point, as an example, we show in Fig 5, the distribution of BR($\widetilde{\chi}_1^\pm \to \widetilde{\chi}_1^0 e^\pm \nu_e$) as a function of $m_{\widetilde{\chi}_1^\pm}$. The different colour codes indicate different regions of the 3-body decay BR($\widetilde{\chi}_2^0 \to \widetilde{\chi}_1^0 e^\pm e^\mp$).

This plot gives an idea of the relative abundance of the three-body decay modes. Note

that if one demands a large BR for the decay mode $\widetilde{\chi}_2^0 \to \widetilde{\chi}_1^0 e^{\pm} e^{\mp}$, the right-handed sleptons in the theory need to be lighter than the left-handed ones. Otherwise the invisible decay mode ($\widetilde{\chi}_2^0 \to \nu\bar{\nu}\widetilde{\chi}_1^0$) takes over to suppress this decay mode. On the other hand, $\widetilde{\chi}_1^{\pm}$ being mostly wino-like does not couple strongly to the right-handed sleptons, suppressing the decay $\widetilde{\chi}_1^{\pm} \to \widetilde{\chi}_1^0 e^{\pm} \nu_e$ which now can only occur via off-shell W-boson and the BR can be $\sim$10% at most as can be seen from Fig 5, denoted by the red and black points. However, there exist a large part of the parameter space, where both $\widetilde{\chi}_2^0$ and $\widetilde{\chi}_1^{\pm}$ may have reasonably large BRs into their respective three body decay modes. All the lepton generations combined, these BRs can be formidable. Later in the collider section, we explore such possibilities and find the exclusion limits for this kind of scenarios.

2.3 Impact of $(g-2)_\mu$

Existence of DM and the experimentally observed [29] excess in the muon anomalous magnetic moment over the SM prediction [48–50] remain two of the most robust hints towards BSM physics. The BSM contribution to muon anomalous magnetic moment (defined as Δa_μ) has to fit within the deviation $\Delta a_\mu = (29.3 \pm 9.0) \times 10^{-10}$ [48]. Efforts have been made to explain this excess in the context of various BSM models [24, 25, 30, 51–54]. Within the framework of the MSSM, small slepton and gaugino masses are favoured in order to enhance Δa_μ to the desired range. Thus part of our parameter space is quite relevant from the angle of this anomalous experimental result. In general, most of the SUSY contribution to Δa_μ arises from the chargino-sneutrino loop. However, the neutralino-smuon loop can also provide significant enhancement depending on the choices of left and right-handed smuon mass parameters. In this section, we use the 1σ, 2σ and 3σ allowed ranges of Δa_μ in order to constrain our parameter space further.

In Fig. 6 (left), we show Δa_μ distribution in the $m_{\widetilde{\chi}_1^{\pm}}$ - $m_{\widetilde{\chi}_1^0}$ plane that gives a clear idea of the favoured choices of these masses. As evident, $m_{\widetilde{\chi}_1^{\pm}} > 600$ GeV is not suited well if one intends to take the Δa_μ constraint seriously. A wide range of the LSP mass is allowed for a particular value of $m_{\widetilde{\chi}_1^{\pm}}$, indicating that the LSP in these cases can be either bino, wino or a well mixed bino-wino state. Another very important factor that goes into the calculation of Δa_μ in this framework, is the mass range of the sleptons, specially, $m_{\widetilde{\mu}_L}$. Therefore, in Fig. 6 (right), we show Δa_μ distribution in the $m_{\widetilde{l}_L}$-$m_{\widetilde{\chi}_1^0}$ plane to give a clear idea about the allowed ranges of the $m_{\widetilde{\mu}_L}$. Clearly, the 1σ and 2σ allowed ranges are at most 900 GeV and 1250 GeV respectively depending on the choices of the LSP and chargino masses.

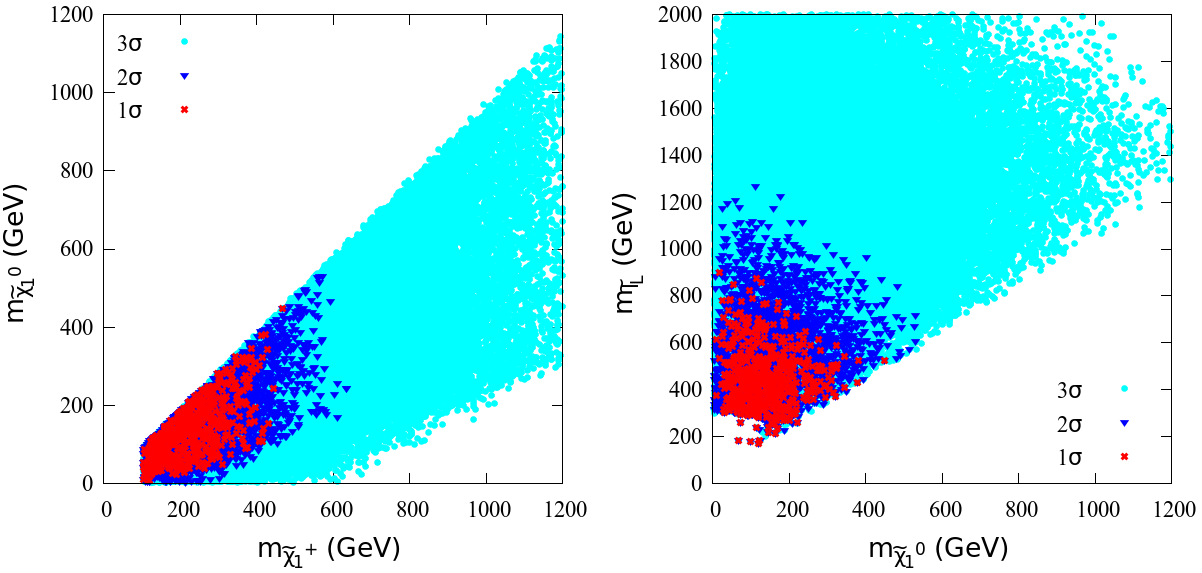

Figure 6: Excess in Δa_μ obtained at 1σ, 2σ and 3σ level shown in the $m_{\widetilde{\chi}_1^\pm}$-$m_{\widetilde{\chi}_1^0}$ and $m_{\widetilde{l}_L}$-$m_{\widetilde{\chi}_1^0}$ plane. The cyan, blue and red points represent 3σ, 2σ and 1σ allowed points respectively.

2.4 Benchmark Points

Based on our discussion so far, we have selected a few benchmark points presented in Table. 1 below. BP1, BP2 and BP3 represent part of the parameter space where two-body decay modes of the electroweakinos are forbidden whereas BP4, BP5 and BP6 represent that where the two-body decays are allowed. Different choices of M_1, M_2, M_{l_L} and M_{l_R} are considered to highlight their effect on the relevant branching ratios and the experimental constraints. For all these benchmark points, squark soft-mass parameters are kept fixed at 3 TeV and a large A_t (4 TeV) is considered in order to fit the SM-like Higgs mass constraint. BP1 and BP2 results in a Δa_μ that lie within its 2σ allowed range. This is mainly because of their light chargino and left-smuon mass. It is hard to achieve this kind of enhancement in Δa_μ once the M_{l_L} parameter starts to increase. This feature can be clearly seen from BP3 and BP5.

BP1 has a large mixing between the bino and wino components. As a result, the $\widetilde{\chi}_2^0 \to \nu\bar{\nu}\widetilde{\chi}_1^0$ decay mode dominates over the $\widetilde{\chi}_2^0 \to l\bar{l}\widetilde{\chi}_1^0$ mode. In BP2 as this mixing decreases, the invisible decay BR starts to fall. In BP3 it becomes negligible as a consequence of having large M_{l_L}. BP4 represents part of the parameter space where the mass gap, $\Delta m^0_{\widetilde{\chi}} = m_{\widetilde{\chi}_2^0} - m_{\widetilde{\chi}_1^0}$ is greater than m_Z but less than m_h and as a result, $\widetilde{\chi}_2^0$ entirely decay into $Z\widetilde{\chi}_1^0$. Once the mass gap increases beyond m_h, the $h\widetilde{\chi}_1^0$ decay mode opens up as shown in BP5. In this case, the

Parameters	BP1	BP2	BP3	BP4	BP5	BP6
M_1	162.4	387.4	352.4	427.3	200.9	177.1
M_2	167.2	411.2	353.3	499.3	380.9	518.3
M_3	2000.0	2000.0	2000.0	2000.0	2000.0	2000.0
μ	334.4	822.3	706.6	998.7	761.8	736.6
$\tan\beta$	13.2	35.7	24.7	20.6	8.9	20.5
M_{l_L}	195.9	437.3	1840.2	785.5	1129.8	1026.4
M_{l_R}	929.3	1048.9	376.5	1024.2	1055.5	586.9
m_h	126.1	125.7	125.6	124.7	123.7	123.5
$m_{\tilde{l}_L}$	201.0	439.6	1840.7	186.8	1130.7	1027.3
$m_{\tilde{l}_R}$	930.3	1049.8	379.1	1025.1	1056.4	588.6
$m_{\tilde{\tau}_1}$	200.9	436.4	378.8	785.1	1056.2	587.9
$m_{\tilde{\tau}_2}$	930.3	1051.2	1840.8	1026.3	1130.9	1028.2
$m_{\tilde{\nu}_L}$	185.5	432.7	1839.1	782.9	1128.1	1027.7
$m_{\widetilde{\chi}_1^0}$	149.6	376.9	346.1	418.6	196.4	173.4
$m_{\widetilde{\chi}_2^0}$	167.4	426.6	370.5	519.9	395.5	531.7
$m_{\widetilde{\chi}_1^\pm}$	163.3	426.4	370.0	519.8	395.4	531.7
$\mathrm{BR}(\widetilde{\chi}_2^0 \to \mathrm{h}\widetilde{\chi}_1^0)$	-	-	-	-	0.94	0.83
$\mathrm{BR}(\widetilde{\chi}_2^0 \to \mathrm{Z}\widetilde{\chi}_1^0)$	-	-	-	1.0	0.06	0.17
$\mathrm{BR}(\widetilde{\chi}_2^0 \to \mathrm{l}\bar{\mathrm{l}}\widetilde{\chi}_1^0)$	1.4×10^{-3}	0.20	0.64	-	-	-
$\mathrm{BR}(\widetilde{\chi}_2^0 \to \tau\bar{\tau}\widetilde{\chi}_1^0)$	4.8×10^{-3}	0.14	0.30	-	-	-
$\mathrm{BR}(\widetilde{\chi}_2^0 \to \nu\bar{\nu}\widetilde{\chi}_1^0)$	0.87	0.63	1.07×10^{-2}	-	-	-
$\mathrm{BR}(\widetilde{\chi}_1^\pm \to \mathrm{W}^\pm\widetilde{\chi}_1^0)$	-	-	-	1.0	1.0	1.0
$\mathrm{BR}(\widetilde{\chi}_1^\pm \to \mathrm{l}\nu\widetilde{\chi}_1^0)$	0.34	0.46	0.22	-	-	-
$\mathrm{BR}(\widetilde{\chi}_1^\pm \to \tau\nu\widetilde{\chi}_1^0)$	0.16	0.25	0.11	-	-	-
$\Delta a_\mu \times 10^{10}$	31.26	15.45	0.80	4.49	1.56	3.72
$\mathrm{BR}(\mathrm{b} \to \mathrm{s}\gamma) \times 10^4$	3.37	3.42	3.40	3.38	3.36	3.39
$\mathrm{BR}(\mathrm{B_s} \to \mu\mu) \times 10^9$	3.01	2.68	2.90	2.94	3.02	2.95

Table 1: Low scale input parameters and the relevant sparticle masses along with the values of the relevant branching ratios and constraints for some of the chosen benchmark points satisfying all the collider, DM and low energy constraints discussed in this section. All the mass parameters are written in GeV unit.

relative branching ratios of these two channels depend upon the abundance of the higgsino component in both $\widetilde{\chi}_1^0$ and $\widetilde{\chi}_2^0$. BP6 has a relatively smaller μ-parameter than BP5 and as a result, has a greater branching ratio into $Z\widetilde{\chi}_1^0$ mode than in BP5. For BP4, BP5 and BP6, $\widetilde{\chi}_1^\pm$ entirely decays into $W^\pm\widetilde{\chi}_1^0$.

3 Collider Analysis

ATLAS and CMS collaborations have presented their search results [16, 19, 22] for direct pair production of $\widetilde{\chi}_1^\pm\widetilde{\chi}_2^0$ mainly in three types of simplified models: (i) *Slepton mediated simplified model*: In such scenarios sleptons are assumed to be lighter than $\widetilde{\chi}_1^\pm$ and $\widetilde{\chi}_2^0$ and the electroweakinos decay via slepton to lepton enriched final states [16]. (ii) *WZ mediated simplified model* : For these types of models sleptons are assumed to be decoupled and the electroweakinos decay via real or virtual gauge bosons ($\mathrm{BR}(\widetilde{\chi}_1^\pm \to W\widetilde{\chi}_1^0) = \mathrm{BR}(\widetilde{\chi}_2^0 \to Z\widetilde{\chi}_1^0) = 100\%$) [16] (iii) *Wh mediated simplified model* : In these scenarios also sleptons are decoupled from the rest of the electroweak sector and the limits are obtained with the assumption that $\mathrm{BR}(\widetilde{\chi}_2^0 \to h\widetilde{\chi}_1^0)$ is 100% [19]. For *WZ mediated simplified model* ATLAS and CMS has looked for trilepton final states with or without τ-tagging [16, 22]. For *Wh mediated simplified model* they have looked for final states consisting of an isolated electron or muon with large $\not{E}_{\mathrm{T}}$ associated with any one of the three following possibilities: two b-tagged jets ($lb\bar{b}$ channel), two photons ($l\gamma\gamma$ channel) or a second electron or muon of similar electric charge ($l^\pm l^\pm$ channel) [19]. Also ATLAS has presented mass limits on $m_{\widetilde{\chi}_1^\pm}$ and $m_{\widetilde{\chi}_2^0}$ considering $h \to \tau\tau, WW, ZZ$ decay modes contributing to trilepton final states: $3l$ ($l = e, \mu$) + 0τ, $2l$+ 1τ, $1l$ + 2τ [16]. Below we briefly discuss about these search analyses [16, 19] used by ATLAS and present our results alongside theirs for validation. Note that, in this work, we have only considered the ATLAS analyses.

3.1 Search for Trilepton final states

Among all the trilepton channels, the exclusion limit obtained by ATLAS is the strongest in $\widetilde{\ell}_L$-mediated model, while that from WZ- and $\widetilde{\tau}_L$-mediated are somewhat similar and weaker. *Wh mediated simplified model* has the weakest limits. Results are also interpreted in few pMSSM scenarios but with fixed values of LSP masses [16]. For validation purpose, we only look into the $\widetilde{\ell}_L$- *and* WZ*-mediated simplified models.* In $\widetilde{\ell}_L$*-mediated* models, left handed sleptons and sneutrinos are assumed to have mass = $(m_{\widetilde{\chi}_1^\mp} + m_{\widetilde{\chi}_2^0})/2$ and the electroweakinos decay either to left handed sleptons or sneutrinos universally. In *WZ mediated simplified*

model , all the sleptons and sneutrinos are assumed to be heavy while the $\widetilde{\chi}_1^{\pm}$ and $\widetilde{\chi}_2^0$ decay via real or virtual W and Z respectively with 100 % BRs.

Events are selected with exactly three tagged leptons (electron, muon or tau) with the requirement that one of these tagged leptons must be either electron or muon[5]. Event reconstruction details like electron, muon, tau and jet identification, isolation, overlap removal etc. are followed according to the ATLAS analysis as mentioned in Sec. 5 of [16]. In this trilepton analysis, a veto on b-jet is applied to all signal channels. For b-jets, we use the p_T dependent b-tagging efficiencies obtained by ATLAS collaboration in Ref. [55]. For τ-jet identification, we only use the hadronic decay modes. We demand that the candidate jets must have $p_T > 20$ GeV and lie within $|\eta| < 2.5$. We also demand that these candidate jets must contain one or three charged tracks with $|\eta_{\rm track}| < 2.5$ and highest track must have $p_T > 3$ GeV. Moreover, in order to ensure proper charge track isolation, we put a veto on any other charged tracks with $p_T > 1$ GeV inside the candidate jet.

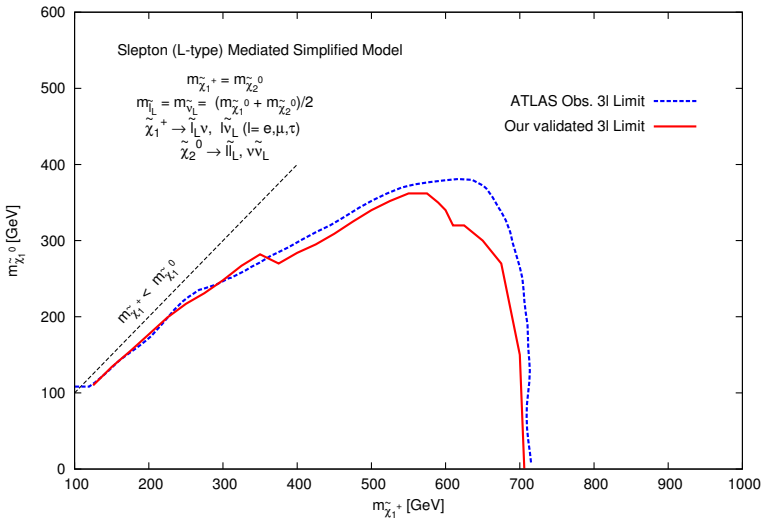

Figure 7: *Validation of ATLAS trilepton + $\not{E}_{\rm T}$ [16] analysis for slepton mediated simplified models. The blue dotted line corresponds to 95 % CL exclusion limits obtained by ATLAS and the solid red line corresponds to our validated results.*

Depending upon the requirement of number of τ-jets ATLAS has defined five signal regions (SR), namely, SR0τa, SR0τb, SR1τ, SR2τa, SR2τb. For implementation of all these signal regions we follow the selection requirements as described in Table 3 and Table 4 of Ref. [16]. Lack of any BSM signal so far in all these channels have resulted in exclusion

[5]Note that here we are not interested in trilepton final states comprising of two or more τ-leptons mostly because of their less significant results in terms of exclusion limits.

limits presented at the 95% confidence level (CL), on the number of BSM signal events, N_{BSM}, for each of the signal regions (SR). These upper limits are presented in Table 7 and Table 8 of Ref [16]. The ATLAS collaboration has translated these obtained upper limits on N_{BSM} into exclusion limits in the $m_{\widetilde{\chi}_1^0}$ - $m_{\widetilde{\chi}_1^\pm}$ plane. In a similar way, we also have reproduced the exclusion contours obtained by ATLAS assuming similar mass relations and branching ratios of the relevant gauginos and sleptons. Note that we have also validated the cut-efficiency table provided by ATLAS. In order to validate our results we reproduce the exclusion contours using PYTHIA (v6.428) [56]. We use the next-to-leading order (NLO) + next-to-leading logarithmic (NLL) chargino-neutralino pair production cross-sections given in Ref. [57], which have been calculated for 8 TeV using the resummino code [58].

We observed that for *slepton, WZ or Wh mediated simplified models*, SR0τa and SR0τb are the most sensitive channels to provide the exclusion limits. Henceforth we will not discuss about the rest of the three signal regions. Depending upon the invariant mass of same-flavour opposite-sign (SFOS) lepton pair (m_{SFOS}), which lies closest to the Z boson mass, SR0τa signal regions are sliced into five bins and each m_{SFOS} slice is further divided into four bins according to the values of $\not{E}_{\rm T}$ and transverse mass, m_T. Here, m_T is constructed with the lepton not forming the SFOS pair and $\not{E}_{\rm T}$.[6] For *slepton mediated models*, SR0τa-bin20 is the most sensitive channel for the parameter space with large mass splitting between $\widetilde{\chi}_1^\pm$ and $\widetilde{\chi}_1^0$ ($\delta m = m_{\widetilde{\chi}_1^\pm} - m_{\widetilde{\chi}_1^0}$). For small δm, low-valued m_{SFOS} SR0τa bins are more effective to probe the relevant parameter space. In Fig. 7, we present the validated results for *slepton mediated simplified models*. The blue dotted line corresponds to 95 % CL exclusion limits obtained by ATLAS and the solid red line corresponds to our validated results adopting the ATLAS analysis. From Fig. 7, it is evident that our validated results are in well agreement with that of ATLAS and for low $m_{\widetilde{\chi}_1^0}$ (< 100 GeV) the trilepton channel excludes chargino masses upto 700 GeV.

For *WZ mediated simplified models*, the upper limits on $m_{\widetilde{\chi}_1^\pm}$ is relatively weaker ($m_{\widetilde{\chi}_1^\pm}$ upto 350 GeV are excluded for massless $\widetilde{\chi}_1^0$). Again for small δm, SR0τa-bin01 offers the best sensitivity and for large δm, the exclusion limits are obtained via SR0τa-bin16. In Fig. 8, we compare the 95% CL exclusion limit obtained by ATLAS (blue dotted line) with the same obtained from our setup (red solid line) and they are in good agreement. It may be noted that the exclusion line in the regions with $m_{\widetilde{\chi}_2^0}(m_{\widetilde{\chi}_1^\pm}) - m_{\widetilde{\chi}_1^0} < m_Z$ (m_W) is obtained from the three body decay of $\widetilde{\chi}_2^0$ ($\widetilde{\chi}_1^\pm$) via off-shell gauge bosons.

[6] For a summary of these 20 bins or 20 SR0τa signal regions, see table 4 of [16].

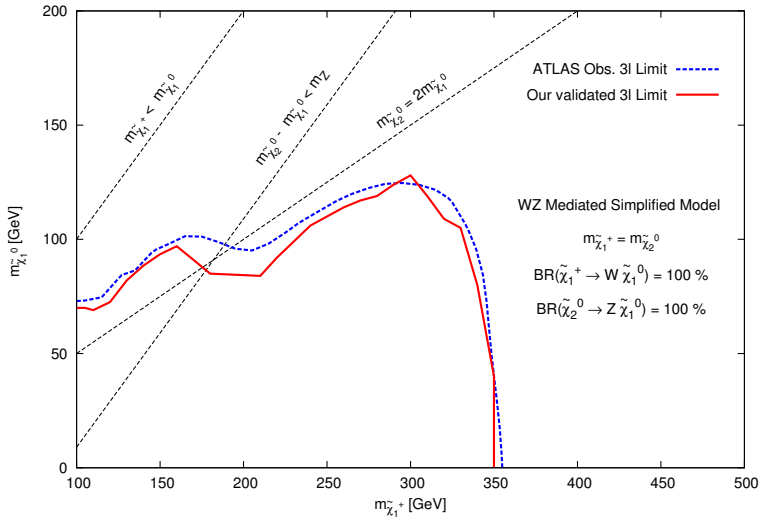

Figure 8: Validation of ATLAS trilepton + $\not{E}_{\rm T}$ [16] analysis for *WZ mediated simplified models*. The blue dotted line corresponds to 95 % CL exclusion limits obtained by ATLAS and the solid red line corresponds to our validated results.

3.2 Search for final states with Higgs

For *Wh mediated simplified models*, where the $\widetilde{\chi}_2^0$ decays into the SM-like Higgs boson and the LSP, ATLAS has very recently presented their results in two new channels [19]. Along with large $\not{E}_{\rm T}$ and an isolated lepton (electron or muon), they have looked for either two b-jets or two photons originating from the 125 GeV Higgs. Here we have considered these two decay modes of the SM-like Higgs since $h \to b\bar{b}$ has the largest branching ratio of all the decay modes of h and although the $BR(h \to \gamma\gamma)$ is usually very small, the large photon detection efficiency makes this decay mode one of the most viable ones in collider studies. We ignore the possible dilepton final state as mentioned in the last section, since it gives the weakest limit on the gaugino masses. We now discuss about our validation results in these two channels.

3.2.1 One lepton and two b-jets channel

In this channel, the events are selected with exactly one lepton with $p_T > 25$ GeV. We also implement all the isolation criteria used by ATLAS to improve the purity of the reconstructed objects and the overlap removal procedure between lepton-lepton or lepton-jets summarised in Table 2 of of Ref [19]. In addition to the charged lepton, the events must contain two or three central jets. We further ensure that there are exactly two 'b-jets' in the final state and

they must be the two hardest central jets. While tagging the b-jets, we have implemented p_T dependent b-tagging efficiency as described in [55]. Dominant background contributions to this final state are expected to arise from $t\bar{t}$, W + jets and single-top Wt production. A large fraction of these SM background events can be suppressed by large missing energy requirement. Most dominant $t\bar{t}$ background can be further suppressed by a suitable cut on the contranverse mass, m_{CT} [59, 60] of the b-jet pair, defined as

$$m_{CT} = \sqrt{(E_T^{b_1} + E_T^{b_2})^2 - |\vec{p_T}^{\,b_1} - \vec{p_T}^{\,b_2}|^2},$$

where, $E_T^{b_i}$ and $\vec{p_T}^{\,b_i}$ are the transverse energy and momentum of the i-th b-jet. Finally, depending upon the values of W transverse mass ($m_T^W = \sqrt{2E_T^l \not{E}_{\rm T} - 2\vec{p_T}^{\,l}.\vec{\not{p}}_{\rm T}}$, where E_T^l and $\vec{p_T}^{\,l}$ are the transverse energy and momentum of the isolated lepton) ATLAS collaboration has defined two signal region: SRlbb-1 which is sensitive to low mass splitting between $m_{\widetilde{\chi}_2^0}$ and m_h and SRlbb-2 which is sensitive to large mass splitting between $m_{\widetilde{\chi}_2^0}$ and m_h. Details of the selection requirement of SRlbb-1 and SRlbb-2 signal regions are enlisted in Table 2. In absence of any excess in this channel, ATLAS collaboration has derived an upper limit on the number of BSM signal events [19] which are quoted in the last row of Table 2.

	SRlbb-1	SRlbb-2
N_{lepton}	1	1
N_{jet}	2-3	2-3
N_{b-jet}	2	2
$\not{E}_{\rm T} >$ (GeV)	100	100
m_{CT} (GeV)	>160	>160
m_T^W	100 - 130	>130
Observed upper limits on N_{BSM} (95 % CL)	5.3	5.5

Table 2: Selection requirements and 95 % upper limit on the number of events at 8 TeV with $\mathcal{L} = 20.3$ fb^{-1} for SRlbb-1 and SRlbb-2 signal regions

In Fig. 9, we reproduce the the exclusion contour in $m_{\widetilde{\chi}_1^0}$ - $m_{\widetilde{\chi}_1^\pm}$ plane obtained by ATLAS with 95% CL using 8 TeV data [19]. In a similar manner described in Sec. 3.1 we validate our simulations. The red dotted line corresponds to ATLAS and the red thick line corresponds to our validated results. From Fig. 9, it is clear that the exclusion line obtained by us is pretty similar to that of ATLAS.

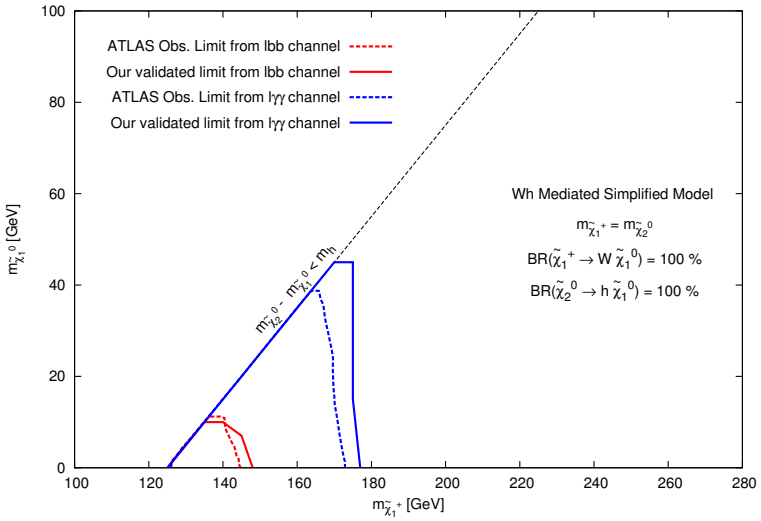

Figure 9: Validation of ATLAS $lbb + \not{E}_{\mathrm{T}}$ and $l\gamma\gamma + \not{E}_{\mathrm{T}}$ [16] analyses for *Wh mediated simplified models*. The blue dotted and solid lines correspond to the 95 % CL exclusion limits obtained by ATLAS and our validated results respectively corresponding to $l\gamma\gamma + \not{E}_{\mathrm{T}}$ final state. Similarly, the red dotted and solid lines represent the experimental bound and our validated results corresponding to $lbb + \not{E}_{\mathrm{T}}$ final state.

3.2.2 One lepton and two photons channel

As already mentioned, the other channel that ATLAS collaboration has also considered while looking for *Wh mediated simplified models*, consists of events with exactly one charged-lepton and two photons in the final state. The events are selected either with single-lepton or with di-photon trigger. For the single-lepton trigger, events are required to have isolated leptons with with $p_T^l > 25$ GeV ($l = e$ or μ) and two leading photons with $p_T^{\gamma 1} > 40$ GeV (leading) and $p_T^{\gamma 2} > 20$ GeV (subleading). For diphoton trigger, the event selection requires p_T thresholds of 15 (10) GeV for electrons (muons), and 40 (27) GeV for the leading (sub-leading) photon. The most dominant background contributions to this channel come from multi-jet and $Z\gamma$ production, where the leptons or jets may be mistagged as photons. An optimum $\not{E}_{\mathrm{T}} > 40$ GeV cut helps to suppress these backgrounds. While reconstructing the $\vec{p_T}$ of the $W \rightarrow l\nu$ system, it is assumed that $\vec{p_T}$ of the neutrino is same as $\vec{\not{p}}_{\mathrm{T}}$ and that it is back to back with the $h \rightarrow \gamma\gamma$ candidate ($\delta\phi(W, h) > 2.25$). These events are divided into two SRs (SR$\ell\gamma\gamma$-1 and SR$\ell\gamma\gamma$-2) based on the values of the transverse mass of the $W\gamma_i$ system, $m_T^{W\gamma_i}$, defined as

$$m_T^{W\gamma_i} = \sqrt{(m_T^W)^2 + 2E_T^W E_T^{\gamma_i} - 2\vec{p_T}^{\,W}.\vec{p_T}^{\,\gamma_i}},$$

where, m_T^W, E_T^W and $\vec{p_T}^W$ are respectively the transverse mass, energy and momentum of W and $E_T^{\gamma_i}$ and $\vec{p_T}^{\gamma_i}$ are the transverse energy and momentum of the i-th photon. All the cuts [19] applied for these two different signal regions are listed in Table 3. Following the same

	SR$l\gamma\gamma$-1	SR$l\gamma\gamma$-2
N_{lepton}	1	1
N_γ	2-3	2-3
$\not{E}_{\rm T}$ > (GeV)	40	40
$\delta\phi(W,h)$ (GeV)	>160	>160
$m_{\gamma\gamma}$ range (GeV)	[100,160]	[100,160]
$m_T^{W\gamma_1}$ and $m_T^{W\gamma_2}$	>150 and >80	<150 or <80
Observed upper limits on N_{BSM} (95 % CL)	3.6	7.0

Table 3: Selection requirements and 95 % upper limit on the number of events at 8 TeV with $\mathcal{L} = 20.3$ fb^{-1} for SR$l\gamma\gamma$-1 and SR$l\gamma\gamma$-2 signal regions

procedure (discussed in previous subsection), we have validated the exclusion limit obtained by ATLAS for Wh simplified scenarios. We present the results in Fig. 9. As evident, our validated results (solid blue line) are in good agreement with the ATLAS exclusion line (blue dotted line).

3.3 Revisiting the exclusion limits with varying branching ratios

In this section, we revisit the aforementioned search channels varying the relevant branching ratios into a particular decay mode to study their impact on the existing exclusion limits provided by the experimental collaborations as discussed in the previous subsection. Quite obviously, the limits are expected to get weaker if one considers shared decay modes of the electroweakinos instead of assuming their wholesome decay into one particular decay mode. For example, in *Wh* and *WZ mediated simplified models* it is assumed that the branching ratios, $\widetilde{\chi}_2^0 \to h\widetilde{\chi}_1^0$ and $Z\widetilde{\chi}_1^0$ are 100% respectively. But in Sec. 2 we have shown that in the allowed kinematic region (see Fig. 1) these two decay modes can compete with each other. Our aim is to assess how much one may expect the exclusion limits to change under such more

realistic situations. We also consider the scenario where electroweakinos are kinematically

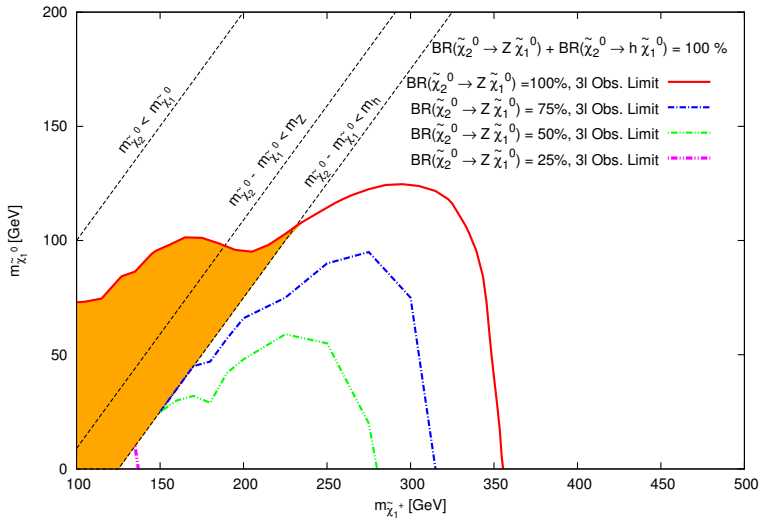

Figure 10: The exclusion lines shown in $m_{\widetilde{\chi}_1^0}$ - $m_{\widetilde{\chi}_1^\pm}$ mass plane for trilepton final state with different choices of BR($\widetilde{\chi}_2^0 \to Z\widetilde{\chi}_1^0$). The red line represents the present experimental bound, whereas the blue, green and magenta dotted lines present our results obtained assuming BR($\widetilde{\chi}_2^0 \to Z\widetilde{\chi}_1^0$) = 75%, 50% and 25% respectively. The black dotted lines separate various kinematic regions where one particular decay mode ceases to exist and another opens up. The yellow shaded region represents the parameter space where either $\widetilde{\chi}_2^0 \to h\widetilde{\chi}_1^0$ or $\widetilde{\chi}_2^0 \to Z\widetilde{\chi}_1^0$ or both these decay modes are forbidden.

forbidden to decay into real W/Z. Under such circumstances, we observe that there exist a large part of the parameter space where the charged sleptons are heavier than $\widetilde{\chi}_2^0$ and $\widetilde{\chi}_1^\pm$, but not so heavy so that they may be considered to be decoupled from the rest of the spectrum, the off-shell decays of the gauginos provide exclusion limits much stronger than that obtained from the usual two-body decay modes.

For the sake of simplicity, first we choose a simplified model where the two body decay modes of $\widetilde{\chi}_2^0$ (wino-like) are varied. We assume that BR($\widetilde{\chi}_2^0 \to Z\widetilde{\chi}_1^0$) + BR($\widetilde{\chi}_2^0 \to h\widetilde{\chi}_1^0$) = 100%, which is true in general if the sleptons are heavier than $\widetilde{\chi}_2^0$. Then for illustrative purpose, we derive the revised limit for BR($\widetilde{\chi}_2^0 \to Z\widetilde{\chi}_1^0$) = 75%, 50% and 25% respectively. In Fig. 10 we present the effect of decreasing $Z\widetilde{\chi}_1^0$ branching ratios over the trilepton final states.

The red solid line represents the exclusion line obtained for *WZ mediated simplified models* with 100% BR to WZ[7] from trilepton modes (the same line from Fig. 8), while the

[7]The sleptons being heavier, the only two-body decay mode available to $\widetilde{\chi}_1^\pm$ is $W^\pm\widetilde{\chi}_1^0$.

blue, green and magenta dotted line represent the exclusion contours for BR($\widetilde{\chi}_2^0 \to Z\widetilde{\chi}_1^0$) = 75%, 50% and 25% respectively. It is clear that the limits reduce drastically due to enhancement of $\widetilde{\chi}_2^0 \to h\widetilde{\chi}_1^0$ decay. The black dotted lines separate different kinematical regions of interest as indicated in the plot. The yellow shaded region is the kinematical region where the trilepton bound is obtained from solely $\widetilde{\chi}_2^0 \to Z\widetilde{\chi}_1^0$ decay mode (if $m_{\widetilde{\chi}_2^0} - m_{\widetilde{\chi}_1^0} < m_h$) or from three-body decays of $\widetilde{\chi}_2^0$ (if $m_{\widetilde{\chi}_2^0} - m_{\widetilde{\chi}_1^0} < m_Z$) via off-shell Z. Note that the trilepton limit almost vanish for BR($\widetilde{\chi}_2^0 \to Z\widetilde{\chi}_1^0$) = 25%.

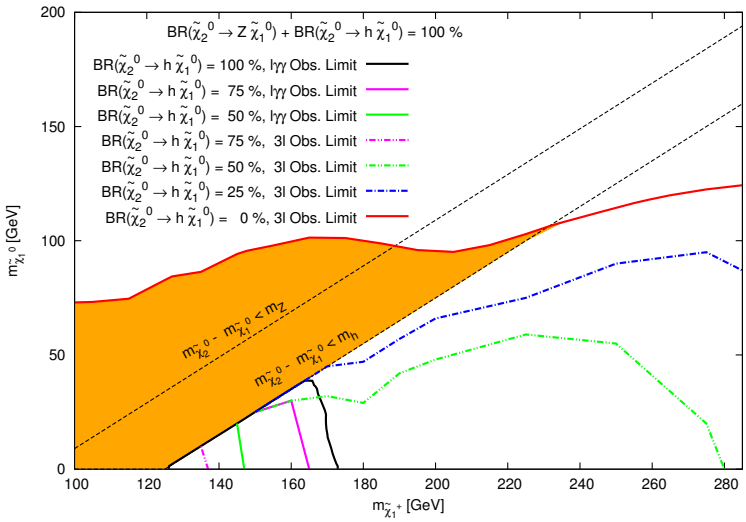
BR(χ̃2 0 → Z χ̃1 0) + BR(χ̃2 0 → h χ̃1 0) = 100 %
BR(χ̃2 0 → h χ̃1 0) = 100 %, lγγ Obs. Limit
BR(χ̃2 0 → h χ̃1 0) = 75 %, lγγ Obs. Limit
BR(χ̃2 0 → h χ̃1 0) = 50 %, lγγ Obs. Limit
BR(χ̃2 0 → h χ̃1 0) = 75 %, 3l Obs. Limit
BR(χ̃2 0 → h χ̃1 0) = 50 %, 3l Obs. Limit
BR(χ̃2 0 → h χ̃1 0) = 25 %, 3l Obs. Limit
BR(χ̃2 0 → h χ̃1 0) = 0 %, 3l Obs. Limit
m χ̃1 0 [GeV]
m χ̃1 ± [GeV]
m χ̃2 0 - m χ̃1 0 < mZ
m χ̃2 0 - m χ̃1 0 < mh
0
50
100
150
200
100
120
140
160
180
200
220
240
260
280

Figure 11: The exclusion lines shown in $m_{\widetilde{\chi}_1^0}$ - $m_{\widetilde{\chi}_1^\pm}$ mass plane for $l\gamma\gamma$ and trilepton final states with different choices of BR($\widetilde{\chi}_2^0 \to h\widetilde{\chi}_1^0$). The solid black line represents the present experimental bound for $l\gamma\gamma$ final state, whereas the solid magenta and solid green lines present our results obtained assuming BR($\widetilde{\chi}_2^0 \to h\widetilde{\chi}_1^0$) = 75% and 50% respectively. The solid red, dotted blue, dotted green and dotted magenta colored lines are the same as shown in Fig. 10.

Next, we concentrate on the decay mode $\widetilde{\chi}_2^0 \to h\widetilde{\chi}_1^0$. In Fig. 11 we present the behaviour of $1l + 2\gamma$ channel where the h decays into two photons[8].

The solid magenta and green lines represent the exclusion limits obtained for BR($\widetilde{\chi}_2^0 \to h\widetilde{\chi}_1^0$) = 75% and 50% whereas the solid black line which is the experimental bound obtained assuming this particular decay BR to be 100%. However, this channel provides much weaker limits compared to the trilepton channel. To showcase this, we have also shown the exclusion lines obtained from the trilepton final states alongside that from $l\gamma\gamma$ final state. The blue and green dotted lines shown in this plot are the same as shown in Fig. 10. Evidently, the

[8] $1l + 2b$ channel provides much weaker limit.

trilepton bounds are stronger unless the BR($\widetilde{\chi}_2^0 \to Z\widetilde{\chi}_1^0$) is close to 25% or smaller. The black dotted lines and the yellow shaded region shown in this plot are the same as in Fig. 10.

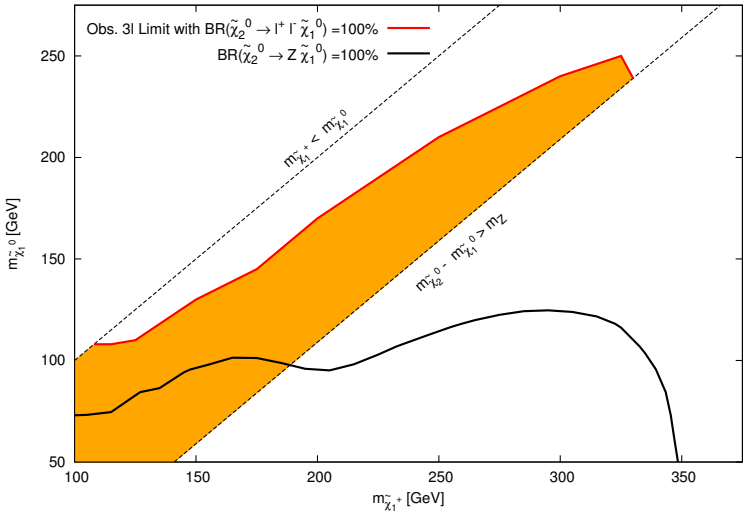

Figure 12: The exclusion lines shown in $m_{\widetilde{\chi}_1^0}$ - $m_{\widetilde{\chi}_1^\pm}$ mass plane for trilepton final state assuming BR($\widetilde{\chi}_2^0 \to l\bar{l}\widetilde{\chi}_1^0$) = 100% and BR($\widetilde{\chi}_1^\pm \to \widetilde{\chi}_1^0 l^\pm \nu_l$) = 30% where $l = e, \mu, \tau$. The solid black line represents the present experimental bound for trilepton final state, whereas the yellow shaded region below the red line shows the obtained exclusion region from trilepton data for such off-shell decays of the electroweakinos.

Finally, we consider the scenario where none of the two-body decays are kinematically allowed for both $\widetilde{\chi}_2^0$ and $\widetilde{\chi}_1^\pm$. Under these circumstances, $\widetilde{\chi}_2^0$ and $\widetilde{\chi}_1^\pm$ may decay via off-shell sleptons[9] and still give rise to the trilepton signal provided the sleptons are not too heavy as can be understood from Fig. 2 and 4. To showcase this, we construct a simplified model motivated by Fig. 5. In this simplified model, $\widetilde{\chi}_2^0$ decays entirely into the three charged lepton pairs universally associated with $\widetilde{\chi}_1^0$, i.e, BR($\widetilde{\chi}_2^0 \to l\bar{l}\widetilde{\chi}_1^0$) = 100% where $l = e, \mu, \tau$. $\widetilde{\chi}_1^\pm$ also decays universally into all its three-body leptonic modes via an off-shell W-boson. However, as indicated in Fig. 5, for a large BR($\widetilde{\chi}_2^0 \to l\bar{l}\widetilde{\chi}_1^0$), the other relevant 3-body BR($\widetilde{\chi}_1^\pm \to \widetilde{\chi}_1^0 l^\pm \nu_l$) remains suppressed. $\widetilde{\chi}_1^\pm$ now decays via an off-shell W-boson and its combined leptonic 3-body BR can be at most 30% Under this scenario, the new exclusion limits obtained from trilepton channel are shown in Fig. 12. The black solid line represents the exclusion line when $\widetilde{\chi}_2^0$ decays only via real or virtual Z. In the region between two dotted black line the two body decay mode via real Z is kinematically not allowed. Now in presence of light slepton we estimate that the whole yellow shaded region under the red solid line are excluded from

[9]Electroweakinos decaying into on-shell sleptons have been studied experimentally. We are not considering that scenario here.

trilepton data. As evident, this limit is much stronger than the conventional one (black line) within the region enclosed by the two dotted black lines.

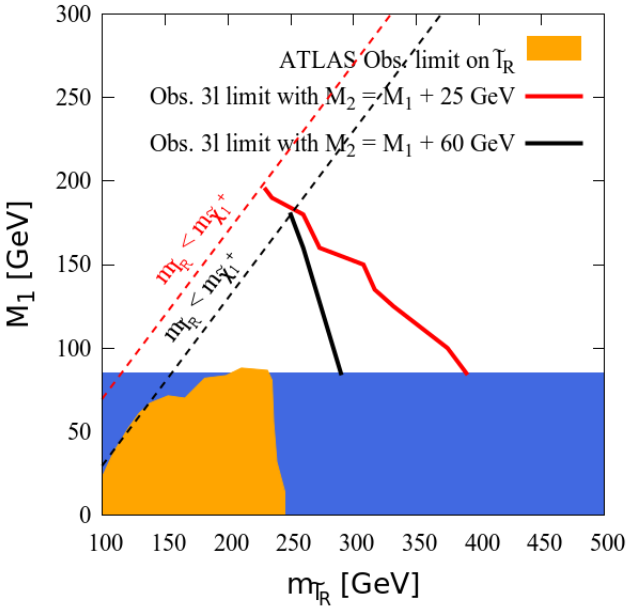

Figure 13: The exclusion lines shown in M_1 - $m_{\tilde{l}_R}$ mass plane for trilepton final state assuming assuming varying branching ratio. The orange region represents the experimental limit on $m_{\tilde{l}_R}$ derived from direct production of the sleptons provided the $m_{\tilde{l}_L}$ are decoupled from the rest of the spectrum. The red and black solid lines correspond to the exclusion lines obtained for $M_2 = M_1$+25 GeV and $M_2 = M_1$+60 GeV respectively. The dotted red and black lines correspond to $m_{\tilde{l}_R} < m_{\tilde{\chi}_1^\pm}$ for the two scenarios: $M_2 = M_1$+25 GeV and $M_2 = M_1$+60 GeV.

In Fig. 13 we show the trilepton exclusion line obtained from off-shell slepton decays keeping M_2 and M_1 at two specific intervals in the M_1-$m_{\tilde{l}_R}$ mass plane for clarity. Note that, unlike Fig. 12, here we do not take a fixed branching ratio of $\widetilde{\chi}_2^0$ and $\widetilde{\chi}_1^\pm$. Instead, we present a more generalised scenario, where this BR may vary freely to give an idea how the exclusion limit applies to the few parameters involved (here the choices being M_1 and $m_{\tilde{l}_R}$) for such decay modes. In Fig. 13 the choice of $M_2 = M_1 + X$ (X chosen such that $m_{\widetilde{\chi}_2^0}$ - $m_{\widetilde{\chi}_1^0} < m_Z$) automatically puts a lower limit on the LSP mass. However, the shaded blue region is the excluded neutralino mass region irrespective of our choice of X since even in the absence of large off-shell slepton decay BR, the contribution arising from off-shell Z-boson decay rules out this part of the parameter space. The dotted red and black lines correspond to $m_{\tilde{l}_R} < m_{\widetilde{\chi}_1^\pm}$ depending upon the choices of X. As expected, $M_2 = M_1$+60 case gives a weaker exclusion limit because of heavier $\widetilde{\chi}_2^0$ and $\widetilde{\chi}_1^\pm$. As X goes down, the exclusion limit

on $m_{\widetilde{l}_R}$ strengthens. However, we chose not to go below 25 GeV, since beyond this limit, the parameter space is highly compressed and the final state leptons are likely to escape detection. This part of the parameter space is clearly visible in Fig. 12 in between the solid red and dotted black line representing $m_{\widetilde{\chi}_1^\pm} < m_{\widetilde{\chi}_1^0}$.

Note that, these limits are comparable to that obtained from l_L-mediated simplified models (see Fig. 7). This implies that even heavier sleptons may result in similar exclusion limits and thereby emphasises the need to probe these off-shell decay modes of the electroweakinos more carefully.

4 Summary and Conclusions

In the absence of any significant results towards the discovery of new physics beyond the SM, the experimental collaborations have extensively studied the obtained data so far to put exclusion limits on the possible BSM scenarios. These experimental limits act as guiding lights toward our quest of BSM physics. However, one has to choose these mass limits judiciously as a lot of simplified assumptions are made in order to obtain such limits. In this work, we have revisited the exclusion limits on the gaugino masses derived from the Run-I data at the LHC. The experimental collaborations have looked into various final states comprised of leptons, jets and missing energy in order to put the exclusion limits in the $m_{\widetilde{\chi}_1^0}$ - $m_{\widetilde{\chi}_1^\pm}$ plane. While deriving these limits, they work with some simplified models where $\widetilde{\chi}_2^0$ and $\widetilde{\chi}_1^\pm$ decay entirely into one of their possible decay modes which although true for some part of the parameter space, often do not present the whole picture. In realistic scenarios, the various decay modes may compete with each other and the exclusion limits are expected to change significantly. Our aim was to assess how much deviation of these exclusion limits one may expect for such scenarios. For that purpose, we have scanned the pMSSM parameter space to find our region of interest where combinations of different decay modes of $\widetilde{\chi}_2^0$ and $\widetilde{\chi}_1^\pm$ may also give rise to the similar final states studied by the experimental collaborations. We show some representative benchmark points obtained from our scan satisfying all the relevant experimental constraints to show the interplay between the branching ratios of the various available decay modes of $\widetilde{\chi}_2^0$ and $\widetilde{\chi}_1^\pm$. We validate our results with those of ATLAS using their assumptions before proceeding to explore the effects of the interplay of the different branching ratios. The obtained results are presented in $m_{\widetilde{\chi}_1^0}$ - $m_{\widetilde{\chi}_1^\pm}$ plane along with the existing experimental results to showcase the significant deviations. We also observe that in the absence of the two-body decay modes, the three-body decays of $\widetilde{\chi}_2^0$ and $\widetilde{\chi}_1^\pm$ via off-shell sleptons can also give rise to the trilepton final states and the exclusion limits obtained are

far more severe than that obtained from off-shell gauge boson decays.

Acknowledgments

The work of AC is supported by the Lancaster-Manchester-Sheffield Consortium for Fundamental Physics under STFC Grant No. ST/L000520/1. The work of SM is partially supported by funding available from the Department of Atomic Energy, Government of India, for the Regional Centre for Accelerator-based Particle Physics (RECAPP), Harish-Chandra Research Institute. The authors also acknowledge useful discussions with Amitava Datta, Utpal Chattopadhyay, Sujoy Poddar and Manimala Chakraborti.

References

[1] G. Aad *et al.* ATLAS Collaboration, Phys. Lett. B **716**, 1 (2012) [arXiv:1207.7214].

[2] S. Chatrchyan *et al.* CMS Collaboration, Phys. Lett. B **716**, 30 (2012) [arXiv:1207.7235].

[3] V. Khachatryan *et al.* [CMS Collaboration], Eur. Phys. J. C **74**, no. 11, 3149 (2014) [arXiv:1207.7235].

[4] G. Aad *et al.* [ATLAS Collaboration], [arXiv:1506.00962];

[5] The ATLAS collaboration, ATLAS-CONF-2015-081.

[6] CMS Collaboration, CMS-PAS-EXO-15-004.

[7] For reviews on supersymmetry, see, *e.g.*, H. P. Nilles, Phys. Rep. **110**, 1 (1984); J. D. Lykken, [arXiv:hep-th/9612114]; J. Wess and J. Bagger, *Supersymmetry and Supergravity*, 2nd ed., (Princeton, 1991).

[8] H. E. Haber and G. Kane, Phys. Rep. **117**, 75 (1985); S. P. Martin, [arXiv:hep-ph/9709356]; D. J. H. Chung *et al.*, Phys. Rept. **407**, 1 (2005) [arXiv:hep-ph/0312378];

[9] M. Drees, P. Roy and R. M. Godbole, *Theory and Phenomenology of Sparticles*, (World Scientific, Singapore, 2005); H. Baer and X. Tata, *Weak scale supersymmetry: From superfields to scattering events*, Cambridge, UK: Univ. Pr. (2006) 537 p.

[10] G. Aad *et al.* [ATLAS Collaboration], JHEP **1409**, 176 (2014) [arXiv:1405.7875]; JHEP **1504**, 116 (2015) [arXiv:1501.03555]; JHEP **1406**, 035 (2014) [arXiv:1404.2500]; G. Aad *et al.* [ATLAS Collaboration], JHEP **1410**, 24 (2014) [arXiv:1407.0600]; [arXiv:1503.03290].

[11] G. Aad *et al.* [ATLAS Collaboration], JHEP **1510**, 134 (2015) [arXiv:1508.06608]; JHEP **1510**, 054 (2015) [arXiv:1507.05525]; Eur. Phys. J. C **75**, no. 10, 510 (2015) [arXiv:1506.08616].

[12] S. Chatrchyan *et al.* [CMS Collaboration], Phys. Lett. B **733**, 328 (2014) [arXiv:1311.4937]. JHEP **1401**, 163 (2014) [JHEP **1501**, 014 (2015)] [arXiv:1311.6736]; JHEP **1406**, 055 (2014) [arXiv:1402.4770]; V. Khachatryan *et al.* [CMS Collaboration], Phys. Lett. B **745**, 5 (2015) [arXiv:1412.4109]; Phys. Rev. D **91**, 052018 (2015) [arXiv:1502.00300]; JHEP **1505**, 078 (2015) [arXiv:1502.04358]; JHEP **1504**, 124 (2015) [arXiv:1502.06031].

[13] T. J. LeCompte and S. P. Martin, Phys. Rev. D **85**, 035023 (2012) [arXiv:1111.6897]; B. Bhattacherjee and K. Ghosh, [arXiv:1207.6289]; H. K. Dreiner, M. Kramer and J. Tattersall, Phys. Rev. D **87**, 035006 (2013) [arXiv:1211.4981]. B. Bhattacherjee, A. Choudhury, K. Ghosh and S. Poddar, Phys. Rev. D **89**, 037702 (2014) [arXiv:1308.1526]; J. Ellis, J. L. Evans, F. Luo and K. A. Olive, JHEP **1602**, 071 (2016) [arXiv:1510.03498]; J. Dutta, P. Konar, S. Mondal, B. Mukhopadhyaya and S. K. Rai, JHEP **1601**, 051 (2016) [arXiv:1511.09284].

[14] G. Aad *et al.* [ATLAS Collaboration], [arXiv:1602.06194]; [arXiv:1602.09058]; The ATLAS collaboration, ATLAS-CONF-2015-076; ATLAS-CONF-2015-077; ATLAS-CONF-2015-078; ATLAS-CONF-2015-082; ATLAS-CONF-2015-067; ATLAS-CONF-2015-066.

[15] V. Khachatryan *et al.* [CMS Collaboration], [arXiv:1602.06581]; CMS Collaboration, CMS-PAS-SUS-15-003; CMS-PAS-SUS-15-004; CMS-PAS-SUS-15-005; CMS-PAS-SUS-15-007; CMS-PAS-SUS-15-008; CMS-PAS-SUS-15-011;

[16] G. Aad *et al.* [ATLAS Collaboration], JHEP **1404**, 169 (2014) [arXiv:1402.7029].

[17] G. Aad *et al.* [ATLAS Collaboration], JHEP **1405**, 071 (2014) [arXiv:1403.5294].

[18] G. Aad *et al.* [ATLAS Collaboration], JHEP **1410**, 96 (2014) [arXiv:1407.0350].

[19] G. Aad *et al.* [ATLAS Collaboration], Eur. Phys. J. C **75**, 208 (2015) [arXiv:1501.07110].

[20] G. Aad *et al.* [ATLAS Collaboration], [arXiv:1509.07152].

[21] V. Khachatryan *et al.* [CMS Collaboration], Phys. Rev. D **90**, 092007 (2014) [arXiv:1409.3168].

[22] V. Khachatryan *et al.* [CMS Collaboration], Eur. Phys. J. C **74**, 3036 (2014) [arXiv:1405.7570].

[23] A. Choudhury and A. Datta, JHEP **09**, 119 (2013) [arXiv:1305.0928]; P. Schwaller and J. Zurita, JHEP **1403**, 060 (2014) [arXiv:1312.7350]; S. P. Das, M. Guchait and D. P. Roy, Phys. Rev. D **90**, no. 5, 055011 (2014) [arXiv:1406.6925]; J. Eckel, M. J. Ramsey-Musolf, W. Shepherd and S. Su, JHEP **1411**, 117 (2014) [arXiv:1408.2841]; C. Han, L. Wu, J. M. Yang, M. Zhang and Y. Zhang, Phys. Rev. D **91**, 055030 (2015) [arXiv:1409.4533]; T. A. W. Martin and D. Morrissey, JHEP **1412**, 168 (2014) [arXiv:1409.6322]; C. Han, [arXiv:1409.7000]; L. Calibbi, J. M. Lindert, T. Ota and Y. Takanishi, JHEP **1411**, 106 (2014) [arXiv:1410.5730]; M. A. Ajaib, B. Dutta, T. Ghosh, I. Gogoladze and Q. Shafi, Phys. Rev. D **92**, no. 7, 075033 (2015) [arXiv:1505.05896].

[24] M. Chakraborti, U. Chattopadhyay, A. Choudhury, A. Datta and S. Poddar, JHEP **1407**, 019 (2014) [arXiv:1404.4841];

[25] M. Chakraborti, U. Chattopadhyay, A. Choudhury, A. Datta and S. Poddar, JHEP **1511**, 050 (2015) [arXiv:1507.01395];

[26] D. Ghosh, M. Guchait and D. Sengupta, Eur. Phys. J. C **72**, 2141 (2012) [arXiv:1202.4937]; K. Howe and P. Saraswat, JHEP **10**, 065 (2012) [arXiv:1208.1542]; A. Arbey, M. Battaglia and F. Mahmoudi, Eur. Phys. J. C **75**, 108 (2015) [arXiv:1212.6865]; T. Han, S. Padhi and S. Su, Phys. Rev. D **88**, 115010 (2013) [arXiv:1309.5966]; A. Papaefstathiou, K. Sakurai and M. Takeuchi, JHEP **1408**, 176 (2014) [arXiv:1404.1077]; F. Yu, Phys. Rev. D **90**, 015009 (2014) [arXiv:1404.2924].

[27] A. Bharucha, S. Heinemeyer and F. von der Pahlen, Eur. Phys. J. C **73**, 2629 (2013) [arXiv:1307.4237].

[28] A. Djouadi *et al.* [MSSM Working Group Collaboration], [hep-ph/9901246].

[29] Muon G-2 Collaboration, Phys. Rev. D73 (2006) 072003 [arXiv:hep-ex/0602035]; B. L. Roberts, Chin. Phys. C34 (2010) 741 [arXiv:1001.2898].

[30] J. Chakrabortty, A. Choudhury and S. Mondal, JHEP **1507**, 038 (2015) [arXiv:1404.2924].

[31] C. Jungman, M. Kamionkowski and K. Griest, Phys. Rep. **267**, 195 (1996) [arXiv:hep-ph/9506380].

[32] G. Bertone, D. Hooper and J. Silk, Phys. Rept. **405**, 279 (2005) [arXiv:hep-ph/0404175];

[33] A. Lahanas, N. Mavromatos and D. Nanopoulos, Int. J. Mod. Phys. D 12, 1529 (2003) [arXiv:hep-ph/0308251]; W. L. Freedman and M. S. Turner, Rev. Mod. Phys. **75**, 1433 (2003) [arXiv:astro-ph/0308418]; L. Roszkowski, Pramana **62**, 389 (2004) [arXiv:hep-ph/0404052]; K. Olive, [arXiv:astro-ph/0503065]; H. Baer and X. Tata, [arXiv:0805.1905], in *Physics at the Large Hadron Collider*, Indian National Science Academy, A Platinum Jubilee Special Issue (Eds. A. Datta, B. Mukhopadhyaya and A. Raychaudhuri; Springer, 2009). M. Drees, [arXiv:1204.2373]; S. Arrenberg *et al.*, [arXiv:1310.8621].

[34] G. Belanger, F. Boudjema, A. Cottrant, R. M. Godbole and A. Semenov, Phys. Lett. B **519**, 93 (2001) [arXiv:hep-ph/0106275]; U. Chattopadhyay, D. Das, P. Konar and D. P. Roy, Phys. Rev. D **75**, 073014 (2007) [arXiv:hep-ph/0610077]; U. Chattopadhyay, D. Das, A. Datta and S. Poddar, Phys. Rev. D **76**, 055008 (2007) [arXiv:0705.0921]; R. M. Godbole, M. Guchait and D. P. Roy, Phys. Rev. D **79**, 095015 (2009) [arXiv:0807.2390]; U. Chattopadhyay and D. Das, Phys. Rev. D **79**, 035007 (2009) [arXiv:0809.4065]; U. Chattopadhyay, D. Das and D. P. Roy, Phys. Rev. D **79**, 095013 (2009) [arXiv:0902.4568]; D. Feldman, Z. Liu, P. Nath and B. D. Nelson, Phys. Rev. D **80**, 075001 (2009) [arXiv:0907.5392]; U. Chattopadhyay, D. Das, D. K. Ghosh and M. Maity, Phys. Rev. D **82**, 075013 (2010) [arXiv:1006.3045]; M. A. Ajaib, T. Li and Q. Shafi, Phys. Rev. D **85**, 055021 (2012) [arXiv:1111.4467]; A. Choudhury and A. Datta, Mod. Phys. Lett. A 27 (2012) 1250188 [arXiv:1207.1846]; S. Mohanty, S. Rao and D. P. Roy, J. High Energy Phys.11 (2012) 175 [arXiv:1208.0894]; M. Chakraborti, U. Chattopadhyay and R. M. Godbole, Phys. Rev. D **87**, no. 3, 035022 (2013) [arXiv:1211.1549]; S. Bhattacharya, S. Chakdar, K. Ghosh and S. Nandi, Phys. Rev. D **89**, 015004 (2014), [arXiv:1309.0036]; K. Harigaya, K. Kaneta and S. Matsumoto, [arXiv:1403.0715], M. Frank and S. Mondal, Phys. Rev. D **90**, no. 7, 075013 (2014) [arXiv:1408.2223]; D. Francescone, S. Akula, B. Altunkaynak and P. Nath, JHEP **1501**, 158 (2015) [arXiv:1410.4999 [hep-ph]]; J. Bramante, P. J. Fox, A. Martin, B. Ostdiek, T. Plehn, T. Schell and M. Takeuchi, Phys. Rev. D **91**, no. 5, 054015 (2015) [arXiv:1412.4789].

[35] S. Akula, D. Feldman, Z. Liu, P. Nath and G. Peim, Mod. Phys. Lett. A 26 (2011) 1521 [arXiv:1103.5061]; N. Bhattacharyya, A. Choudhury and A. Datta, Phys. Rev. D

83, 115025 (2011) [arXiv:1104.0333]; N. Bhattacharyya, A. Choudhury and A. Datta, Phys. Rev. D **84**, 095006 (2011) [arXiv:1107.1997]; K. A. Olive, [arXiv:1202.2324]; D. Ghosh, M. Guchait, S. Raychaudhuri and D. Sengupta, Phys. Rev. D **86**, 055007 (2012) [arXiv:1205.2283]; P. Nath, [arXiv:1207.5501]; J. Ellis, Eur. Phys. J. C **74**, 2732 (2014) [arXiv:1312.5426].

[36] D. A. Vasquez, G. Belanger and C. Boehm, Phys. Rev. D **84**, 095015 (2011) [arXiv:1108.1338]; A. Choudhury and A. Datta, JHEP **06** (2012) 006 [arXiv:1203.4106]; A. J. Williams, C. Boehm, S. M. West and D. A. Vasquez, Phys. Rev. D **86**, 055018 (2012) [arXiv:1204.3727]; G. Belanger, S. Biswas, C. Boehm and B. Mukhopadhyaya, JHEP **1212**, 076 (2012) [arXiv:1206.5404]; G. Arcadi, R. Catena and P. Ullio, [arXiv:1211.5129]; C. Boehm, P. S. B. Dev, A. Mazumdar and E. Pukartas, JHEP **06** (2013) 113 [arXiv:1303.5386]; J. A. Casas, J. M. Moreno, K. Rolbiecki and B. Zaldivar, [arXiv:1305.3274]; B. Bhattacherjee, M. Chakraborti, A. Chakraborty, U. Chattopadhyay, D. Das and D. K. Ghosh, Phys. Rev. D **88** (2013) 035011 [arXiv:1305.4020]; A. Fowlie, K. Kowalska, L. Roszkowski, E. M. Sessolo and Y. L. S. Tsai, Phys. Rev. D **88**, 055012 (2013) [arXiv:1306.1567]; K. Kowalska and E. M. Sessolo, Phys. Rev. D **88**, no. 7, 075001 (2013) [arXiv:1307.5790]; A. Arbey, M. Battaglia and F. Mahmoudi, Phys. Rev. D **88**, 095001 (2013) [arXiv:1308.2153]; A. Pierce, N. R. Shah, K. Freese [arXiv:1309.7351]; K. Kowalska, L. Roszkowski, E. M. Sessolo and S. Trojanowski, JHEP **1404**, 166 (2014) [arXiv:1402.1328]; M. Chakraborti, U. Chattopadhyay, S. Rao and D. P. Roy, Phys. Rev. D **91**, 035022 (2015) [arXiv:1411.4517]; L. Roszkowski, E. M. Sessolo and A. J. Williams, JHEP **1502**, 014 (2015) [arXiv:1411.5214]; A. Chatterjee, A. Choudhury, A. Datta and B. Mukhopadhyaya, JHEP **1501**, 154 (2015) [arXiv:1411.6467]; G. Belanger, D. Ghosh, R. Godbole and S. Kulkarni, [arXiv:1506.00665].

[37] C. Cheung, L. J. Hall, D. Pinner and J. T. Ruderman, JHEP **1305**, 100 (2013) [arXiv:1211.4873]; P. Huang and C. E. M. Wagner, Phys. Rev. D **90**, no. 1, 015018 (2014) [arXiv:1404.0392]; L. Roszkowski, S. Trojanowski and K. Turzyski, JHEP **1411**, 146 (2014) [arXiv:1406.0012]; M. E. C. Catalan, S. Ando, C. Weniger and F. Zandanel, [arXiv:1503.00599].

[38] E. A. Bagnaschi *et al.*, Eur. Phys. J. C **75**, 500 (2015) [arXiv:1508.01173]; K. Hamaguchi and K. Ishikawa, [arXiv:1510.05378]; J. Bramante, N. Desai, P. Fox, A. Martin, B. Ostdiek and T. Plehn, [arXiv:1510.03460]; B. Kaufman, P. Nath, B. D. Nelson and A. B. Spisak, Phys. Rev. D **92**, 095021 (2015) [arXiv:1509.02530]; J. Cao, Y. He,

L. Shang, W. Su and Y. Zhang, [arXiv:1511.05386]; M. Cannoni, J. Ellis, M. E. Gmez, S. Lola and R. R. de Austri, [arXiv:1511.06205]; S. Heinemeyer, [arXiv:1602.08040].

[39] T. Han, Z. Liu and A. Natarajan, JHEP **1311**, 008 (2013) [arXiv:1303.3040].

[40] G. Hinshaw *et al.*, (WMAP Collaboration), [arXiv:1212.5226].

[41] P. A. R. Ade, *et al.*, [Planck Collaboration], [arXiv:1303.5076].

[42] A. Djouadi, J. L. Kneur and G. Moultaka, Comp. Phys. Comm. **176**, 426 (2007) [arXiv:hep-ph/0211331].

[43] A. Djouadi, M. M. Muhlleitner and M. Spira, Acta Phys. Polon. B **38**, 635 (2007) [arXiv:hep-ph/0609292].

[44] G. Belanger, F. Boudjema, A. Pukhov and A. Semenov, Comput. Phys. Commun. **185** (2014) 960 [arXiv:1305.0237].

[45] G. Degrassi, S. Heinemeyer, W. Hollik, P. Slavich and G. Weiglein, Eur. Phys. J. C **28**, 133 (2003) [arxiv:hep-ph/0212020]; B. C. Allanach, A. Djouadi, J. L. Kneur, W. Porod and P. Slavich, JHEP **09**, 044 (2004) [arxiv:hep-ph/0406166]; S. P. Martin, Phys. Rev. D **75**, 055005 (2007) [arxiv:hep-ph/0701051]; R. V. Harlander, P. Kant, L. Mihaila and M. Steinhauser, Phys. Rev. Lett. **100**, 191602 (2008) [arXiv:0803.0672], Erratum: Phys. Rev. Lett. **101**, 039901 (2008); S. Heinemeyer, O. Stal and G. Weiglein, Phys. Lett. B **710**, 201 (2012) [arXiv:1112.3026]; A. Arbey, M. Battaglia, A. Djouadi and F. Mahmoudi, [arXiv:1207.1348].

[46] The LEP SUSY Working Group, http://lepsusy.web.cern.ch/lepsusy/.

[47] Y. Amhis *et al.* [Heavy Flavor Averaging Group (HFAG) Collaboration], [arXiv:1412.7515].

[48] F. Jegerlehner and A. Nyffeler, Phys. Rept. 477 (2009) 1-110 [arXiv:0902.3360].

[49] K. Hagiwara, R. Liao, A. D. Martin, D. Nomura and T. Teubner, J. Phys. G G38 (2011) 085003 [arXiv:1105.3149].

[50] A. Nyffeler, Nuovo Cim. C **037**, no. 02, 173 (2014) [arXiv:1312.4804] and references therein.

[51] D. A. Kosower, L. M. Krauss and N. Sakai, Phys. Lett. B **133**, 305 (1983); T. C. Yuan, R. Arnowitt, A. H. Chamseddine and P. Nath, Z. Phys. C **26**, 407 (1984); J. L. Lopez, D. V. Nanopoulos and X. Wang, Phys. Rev. D **49**, 366 (1994); U. Chattopadhyay and P. Nath, Phys. Rev. D **53**, 1648 (1996) [arXiv:hep-ph/9507386]; U. Chattopadhyay and P. Nath, Phys. Rev. Lett. **86** (2001) 5854 [arXiv:hep-ph/0102157]; U. Chattopadhyay and P. Nath, Phys. Rev. D **66** (2002) 093001 [arXiv:hep-ph/0208012].

[52] S. Mohanty, S. Rao and D. P. Roy, JHEP **09** (2013) 027 [arXiv:1303.5830]; S. Akula and P. Nath, Phys. Rev. D **87** (2013) 115022 [arXiv:1304.5526]; N. Okada, S. Raza and Q. Shafi, arXiv:1307.0461; J. Chakrabortty, S. Mohanty and S. Rao, JHEP **02** (2014) 074 [arXiv:1310.3620]. S. Iwamoto, T. T. Yanagida and N. Yokozaki, [arXiv:1407.4226]; K. Kowalska, L. Roszkowski, E. M. Sessolo and A. J. Williams, JHEP **1506**, 020 (2015) [arXiv:1503.08219].

[53] M. Endo, K. Hamaguchi, S. Iwamoto, T. Yoshinaga, JHEP **01** (2014) 123 [arXiv:1303.4256]; F. Wang, W. Wang and J. M. Yang, JHEP **1506**, 079 (2015) [arXiv:1504.00505]; F. Wang, W. Wang, J. M. Yang and Y. Zhang, JHEP **1507**, 138 (2015) [arXiv:1505.02785]; A. Chakraborty and S. Chakraborty, [arXiv:1511.08874].

[54] L. L. Everett, G. L. Kane, S. Rigolin and L. T. Wang, Phys. Rev. Lett. **86**, 3484 (2001) [arXiv:hep-ph/0102145].

[55] ATLAS Collaboration, ATLAS-CONF-2012-043 [https://cds.cern.ch/record/1435197].

[56] T. Sjostrand, S. Mrenna and P. Skands, JHEP **05** (2006) 026 [arXiv:hep-ph/0603175].

[57] https://twiki.cern.ch/twiki/bin/view/CMSPublic/WinoCn.

[58] B. Fuks, M. Klasen, D. R. Lamprea and M. Rothering, JHEP **1210**, 081 (2012) [arXiv:1207.2159]; B. Fuks, M. Klasen, D. R. Lamprea and M. Rothering, Eur. Phys. J. C **73**, 2480 (2013) [arXiv:1304.0790].

[59] D. R. Tovey, JHEP **0804**, 034 (2008) [arXiv:0802.2879].

[60] G. Polesello and D. R. Tovey, JHEP **1003**, 030 (2010) [arXiv:0910.0174].